changes observed on both sides of the membrane provide a structural basis for the widely held view of an alternating access model deduced from kinetics data.

References and Notes

1. O. Jardetzky, *Nature* **211**, 969 (1966).
2. C. Tanford, *Proc. Natl. Acad. Sci. U.S.A.* **80**, 3701 (1983).
3. H. R. Kaback *et al.*, *Proc. Natl. Acad. Sci. U.S.A.* **104**, 491 (2007).
4. D. D. F. Loo, B. A. Hirayama, M. H. Karakossian, A. K. Meinild, E. M. Wright, *J. Gen. Physiol.* **128**, 701 (2006).
5. C. Toyoshima, *Arch. Biochem. Biophys.* **476**, 3 (2008).
6. K. Hollenstein, R. J. Dawson, K. P. Locher, *Curr. Opin. Struct. Biol.* **17**, 412 (2007).
7. O. Mirza, L. Guan, G. Verner, S. Iwata, H. R. Kaback, *EMBO J.* **25**, 1177 (2006).
8. J. Abramson *et al.*, *Science* **301**, 610 (2003).
9. L. Guan, O. Mirza, G. Verner, S. Iwata, H. R. Kaback, *Proc. Natl. Acad. Sci. U.S.A.* **104**, 15294 (2007).
10. Y. Huang, M. J. Lemieux, J. Song, M. Auer, D. N. Wang, *Science* **301**, 616 (2003).
11. Y. Yin, X. He, P. Szewczyk, T. Nguyen, G. Chang, *Science* **312**, 741 (2006).
12. S. Suzuki, P. J. Henderson, *J. Bacteriol.* **188**, 3329 (2006).
13. M. H. Saier Jr., *Adv. Microb. Physiol.* **40**, 81 (1998).
14. M. H. Saier Jr., C. V. Tran, R. D. Barabote, *Nucleic Acids Res.* **34**, D181 (2006).
15. A. Pantazopoulou, G. Diallinas, *FEMS Microbiol. Rev.* **31**, 657 (2007).
16. Q. Ren, K. Chen, I. T. Paulsen, *Nucleic Acids Res.* **35**, D274 (2007).
17. A. Yamashita, S. K. Singh, T. Kawate, Y. Jin, E. Gouaux, *Nature* **437**, 215 (2005).
18. S. K. Singh, A. Yamashita, E. Gouaux, *Nature* **448**, 952 (2007).
19. Z. Zhou *et al.*, *Science* **317**, 1390 (2007); published online 9 August 2007 (10.1126/science.1147614).
20. L. Shi, M. Quick, Y. Zhao, H. Weinstein, J. A. Javitch, *Mol. Cell* **30**, 667 (2008).
21. S. Faham *et al.*, *Science* **321**, 810 (2008); published online 3 July 2008 (10.1126/science.1160406).
22. E. Turk *et al.*, *J. Biol. Chem.* **275**, 25711 (2000).
23. X. Huang, W. Miller, *Adv. Appl. Math.* **12**, 337 (1991).
24. Materials and methods are available as supporting material on *Science* Online.
25. K. Cowtan, *Joint CCP4 and ESF-EACBM Newsletter on Protein Crystallography* **31**, 34 (1994).
26. P. D. Adams *et al.*, *Acta Crystallogr. D* **58**, 1948 (2002).
27. C. Hunte *et al.*, *Nature* **435**, 1197 (2005).
28. D. Yernool, O. Boudker, Y. Jin, E. Gouaux, *Nature* **431**, 811 (2004).
29. D. Fu *et al.*, *Science* **290**, 481 (2000).
30. R. Dutzler, E. B. Campbell, M. Cadene, B. T. Chait, R. MacKinnon, *Nature* **415**, 287 (2002).
31. J. U. Bowie, *Nat. Struct. Mol. Biol.* **13**, 94 (2006).
32. M. R. Chevallier, R. Jund, F. Lacroute, *J. Bacteriol.* **122**, 629 (1975).
33. J. C. Bloch, H. Sychrova, J. L. Souciet, R. Jund, M. R. Chevallier, *Mol. Microbiol.* **6**, 2989 (1992).
34. D. Brèthes *et al.*, *Eur. J. Biochem.* **204**, 699 (1992).
35. T. Ferreira, D. Brèthes, B. Pinson, C. Napias, J. Chevallier, *J. Biol. Chem.* **272**, 9697 (1997).
36. Single-letter abbreviations for the amino acid residues are as follows: A, Ala; I, Ile; N, Asn; P, Pro; Q, Gln; S, Ser; T, Thr; and W, Trp.
37. P. J. Henderson, G. E. Martin, T. P. McDonald, A. Steel, A. R. Walmsley, *Antonie Leeuwenhoek* **65**, 349 (1994).
38. T. H. Wilson, P. Z. Ding, *Biochim. Biophys. Acta* **1505**, 121 (2001).
39. S. C. Lovell, *Proteins* **50**, 437 (2003).

40. This research was funded primarily by the Biotechnology and Biological Sciences Research Council (grant nos. B17935 and BB/C51725), with important contributions from Ajinomoto Incorporated, the European Membrane Protein consortium (grant no. LSHG-CT-2004-504601), the Membrane Protein Structure Initiative (grant no. BBS/B/14418), and the Wellcome Trust (grant no. 062164/Z/00/Z). We wish to thank the Membrane Protein Laboratory (MPL) at the Diamond Light Source Limited for use of the MPL facilities. J. Abramson kindly provided us with the coordinates of vSGLT before their release from the Protein Data Bank (PDB). We are also grateful to S. Phillips, S. Baldwin, P. Gilmartin, S. Radford, D. Drew, M. Jormakka, K. Watanabe, and M. Iwata for support or advice. The Japan Society for the Promotion of Science provided personal funding to S.Y. and the Leverhulme Trust to P.J.F.H. S.W. was a recipient of a European Molecular Biology Organization long-term fellowship. The coordinates and the structure factors for Mhp1 without substrate and the hydantoin complex have been deposited in the PDB (entries 2JLN and 2JLO, respectively).

Supporting Online Material

www.sciencemag.org/cgi/content/full/1164440/DC1
Materials and Methods
Table S1
Figs. S1 to S8
References

8 August 2008; accepted 26 September 2008
Published online 16 October 2008;
10.1126/science.1164440
Include this information when citing paper.

REPORTS

Magnetism on the Angrite Parent Body and the Early Differentiation of Planetesimals

Benjamin P. Weiss,[1]* James S. Berdahl,[1] Linda Elkins-Tanton,[1] Sabine Stanley,[2] Eduardo A. Lima,[1] Laurent Carporzen[1]

Angrites are among the oldest known pristine basaltic meteorites and record the earliest stages of planet formation and differentiation. Our paleomagnetic analysis of three angrites found that they record a past magnetic field of ~10 microteslas on the angrite parent body extending from 4564 to at least 4558 million years ago. Because the angrite paleomagnetic record extends beyond the expected lifetime of the early circumstellar disk, these paleofields were probably generated internally on the angrite parent body, possibly by an early dynamo in a rapidly formed metallic core.

Basaltic achondrites are thought to be igneous samples of the first differentiated planetary bodies. Several classes of these meteorites have crystallization ages within just ~3 million years (My) of the formation of the solar system and contain geochemical signatures of metal and silicate fractionation. Remanent magnetization has been detected in meteorites from five basaltic achondrite groups, indicating the presence of past magnetic fields on these bodies (*1*). However, these meteorites, as well as nearly all basaltic achondrite groups, were subjected to brecciation, shock, and metamorphic events tens to hundreds of millions of years after their formation that modified and, in many cases, reset their magnetization. Because magnetic fields can be generated by large impacts (*2*), the fields recorded on these bodies also may not have been generated internally.

An exception is the angrites, a group of twelve basaltic achondrites from an as yet unidentified parent body. Angrites have Pb/Pb and Hf/W ages of 4564 to 4558 million years ago (Ma) (*3*–*5*) that are within error of their (U-Th)/He ages for all but two meteorites (*6*). They entirely lack shock, post-cooling brecciation, and parent-body weathering textures (*7*–*12*), which makes them among the best preserved materials known from the early solar system. Angrites may therefore record two fundamental field-generating mechanisms postulated to exist in the early solar system: stellar and circumstellar disk fields external to the angrite parent body (APB) and an internal core dynamo on the APB.

Here we present a paleomagnetic investigation of 3 of the 12 known angrites: Angra dos Reis, D'Orbigny, and Asuka (A) -881371. We found that the angrites Northwest Africa (NWA) 2999 and NWA 4801 have been substantially remagnetized by collectors' hand magnets (as indicated by communication with previous owners of the samples and moments near saturation), whereas NWA 4931 has been heavily weathered

[1]Department of Earth, Atmospheric, and Planetary Sciences, Massachusetts Institute of Technology, 54-814, 77 Massachusetts Avenue, Cambridge, MA 02139, USA. [2]Department of Physics, University of Toronto, 60 St. George Street, Toronto, ON M5S 1A7, Canada.

*To whom correspondence should be addressed. E-mail: bpweiss@mit.edu

since arrival on Earth. Most of the remaining six angrites are either hot desert meteorites (probably subjected to weathering and magnet remagnetization) or not readily available to the scientific community.

Nearly all angrites contain several primary ferromagnetic minerals: low-Ti magnetite (*13*), titanomagnetite [typical composition of 71 to 77 mole percent (mol %) ulvöspinel, with 17 to 21 mol % magnetite] (*14*), and rarer kamacite (typically $Fe_{0.95}Ni_{0.05}$, except for D'Orbigny, which reportedly contains $FeNi_2$) and pyrrhotite (*7*, *14*). Our thermomagnetic, hysteresis, and other rock magnetic data [see the supporting online material (SOM)] indicate that the dominant ferromagnetic mineral in D'Orbigny and A-881371 is pseudo–single domain, low-Ti magnetite. Angra dos Reis contains two pseudo–single domain ferromagnetic minerals, one of which is probably low-Ti magnetite and the other a higher coercivity phase (either sulfide or metal). None of these meteorites exhibits a Verwey transition (see SOM), indicating that the magnetite is not stoichiometric and that any effects from inverse thermoremanent magnetization (ITRM) processes (*15*) must be modest [in any case, the high blocking coercivity of the natural remanent magnetization (NRM) in these meteorites implies that ITRM cannot be a major contributor]. Furthermore, none of these angrites contain appreciable quantities of ferromagnetic weathering minerals (see SOM). Angra dos Reis is particularly pristine because it was quickly recovered after it fell on Earth (*8*, *16*). The well-understood magnetic properties of magnetite mean that, relative to most other meteorites, angrites are very-high-fidelity magnetic recorders.

D'Orbigny is a pristine vesicular basalt containing undevitrified igneous glass (*7*). It is among the oldest known angrites, with final cooling ages only ~3 to 4 My younger than calcium- and aluminum-rich inclusions (CAIs) and the origin of the solar system (*3*, *4*, *17*). D'Orbigny's large size afforded us the opportunity to acquire samples ranging from the fusion crust to the center (150 mm deep) to identify preterrestrial remanence. Alternating field (AF) demagnetization, rock magnetic, and paleointensity studies of mutually oriented subsamples revealed that much of the exterior ~1 mm of the meteorite has been completely remagnetized by the collector's magnet (see SOM). Subsamples at 12 to 30 mm of depth had two main components of magnetization: (i) a nonunidirectional, near saturation, low-coercivity (LC) component from the collector's magnet (typically blocked up to ~5 to 10 mT) and (ii) a high-coercivity (HC) component (blocked up to at least ~40 to >290 mT, depending on the subsample) with a ratio of NRM to saturation isothermal remanent magnetization (IRM) <1%. The HC component trended to the origin and was unidirectional across all mutually oriented interior subsamples (fig. S1), consistent with a primary thermoremanence. Subsamples at $\gtrsim 8$ cm of depth had only a moderate LC overprint varying in intensity between that expected for a terrestrial viscous remanent magnetization and a low-field (<7 mT) IRM (Fig. 1A and fig. S2). Paleointensity experiments (*18*) on HC components from nine subsamples gave paleofield values of 17 ± 6 μT after normalizing to anhysteretic remanent magnetization (ARM) acquired in 50, 200, and 600 μT dc bias fields and 15 ± 5 μT after normalizing to IRM (uncertainties are SDs of values for nine subsamples) (table S3).

A-881371 is a fine-grained ophitic basalt with olivine megacrysts (*13*) and is nearly the same age as D'Orbigny (*5*). AF demagnetization of a single 66-mg grain from the interior of this tiny meteorite (≥5 mm from nearest fusion crust) revealed a LC component up to 7.2 mT (Fig. 1B and fig. S3A). Our magnetic viscosity experiments indicate that this component is almost certainly a viscous remanent magnetization acquired during residence on Earth (see SOM). A weaker HC magnetization is present up to at least 150 mT but does not notably decay in intensity during AF demagnetization due to the relatively high ARM noise from our AF system. AF demagnetization of a laboratory ARM acquired in a 7-μT dc bias field (chosen to yield a similar pa-

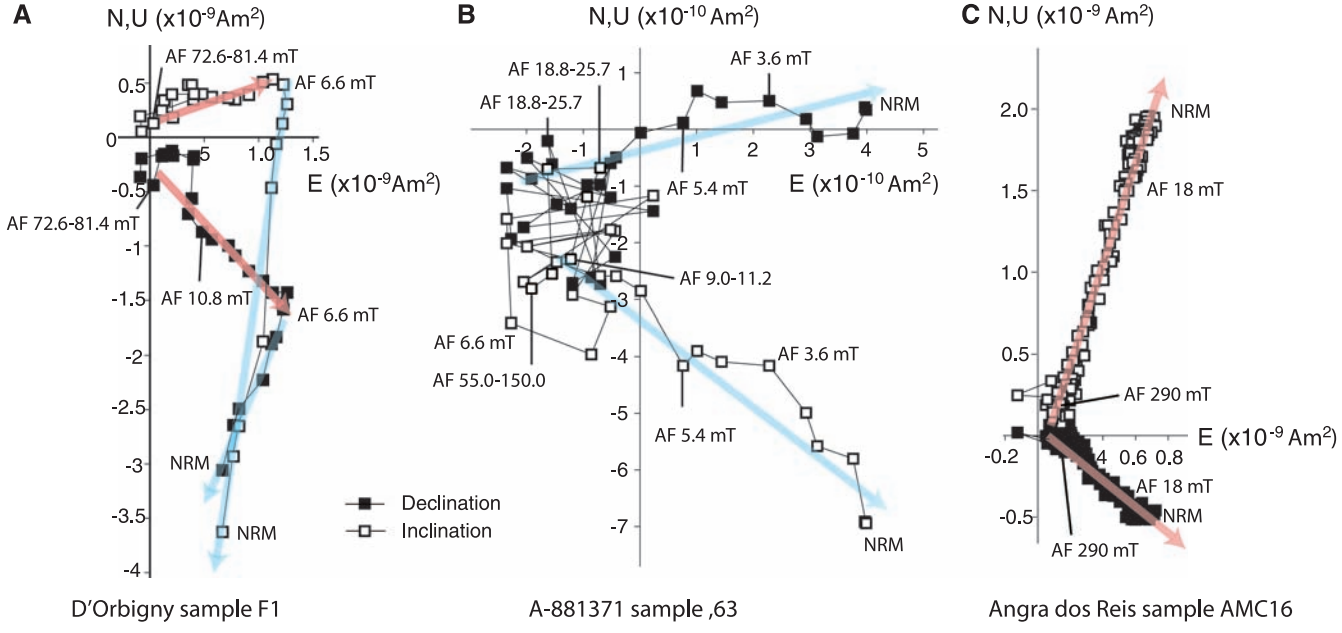

Fig. 1. NRM of angrites. A two-dimensional projection of the endpoint of the NRM vector during AF demagnetization is shown. Closed and open symbols represent end points of magnetization projected onto horizontal N-S-E-W and vertical U-D-E-W planes, respectively. Peak fields for selected AF demagnetization steps are labeled. One or two main components are visible: (i) sometimes a LC component (blue arrow) and (ii) always a HC component (red arrow). (**A**) D'Orbigny interior (~8 cm depth) sample F1. To reduce spurious ARM noise, steps from AF 7.2 to 8.4 mT were averaged over three consecutive steps, and steps from AF 9.0 to 83.6 mT were averaged over five consecutive steps. A least-squares fit to all HC steps without averaging from AF 6.6- to 50.6-mT deviates from the origin by dANG = 6° (calculated by anchoring to the AF 6.6-mT direction), which is less than the fit's uncertainty, represented as the maximum angular deviation (MAD) = 29.5°, consistent with the HC component trending to the origin. (**B**) A-881371 interior sample ,63. Two main components are visible: (i) a LC component (approximate direction given by blue arrow) and (ii) a HC component identified as an offset of the mean direction above AF 9.0 mT from the origin. High-AF directions are averages of multiple AF steps (compare with fig. S3A). (**C**) Angra dos Reis interior sample AMC-16. A least-squares fit to all HC steps without averaging from AF 18 to 74.8 mT gives dANG = 4.5° (anchored to the AF 18-mT direction), which is less than the fit's mean MAD = 5.7°, consistent with the HC component trending to the origin.

leointensity as that of the NRM) exhibits the same high AF-related noise (fig. S3B). If we assume this is the characteristic magnetization, then we obtain paleointensities of ~3 to 8 μT (ARM method) and ~2 μT (IRM method) (fig. S3, C and D, and table S3). D'Orbigny's and A-881371's great age, excellent preservation state, and nearly instantaneous (10 to 50°C hour^{-1}) primary igneous cooling rates (*19*) indicate that their HC magnetization is a truly ancient thermoremanence (*20*).

The coarse-grained younger angrite Angra dos Reis (Pb/Pb age of 4557.7 ± 0.1 Ma) (*3*) also has a preterrestrial magnetization acquired in a similarly substantial magnetic field. Our AF analyses of mutually oriented subsamples from a chip of Angra dos Reis from the American Museum of Natural History (AMNH) traversing the fusion crust to the interior revealed a unidirectional magnetization in the interior. Subsamples from within 2.7 mm of the fusion crust have directions divergent from (coincidentally nearly antipodal to) the interior and Earth-strength paleointensities. This is consistent with the outer few millimeters having been baked by atmospheric passage and indicates that the magnetization in the unbaked interior is preterrestrial (Fig. 2). This interior magnetization consisted of a HC primary magnetization component (extending from 15.8 to >290 mT) trending to the origin (Fig. 1C), usually overprinted by a weak LC component that is probably a terrestrial VRM (see SOM). AF demagnetization of five mutually oriented subsamples of a second chip of Angra dos Reis taken from the interior (≥6 mm from the nearest fusion crust) of the main mass in Museu Nacional, Brazil (MNB) revealed an intense LC overprint from previous sample handling and a unidirectional HC component trending to the origin interpreted as a primary thermoremanence (fig. S1). Two additional subsamples on the opposite side of the chip were nearly fully overprinted by the high intensity component and did not yield primary remanence. Paleointensity experiments on the HC component for seven subsamples from both the AMNH and MNB samples gave mean values and SDs of 17 ± 11 μT (ARM method) and 19 ± 9 μT (IRM method) (table S3).

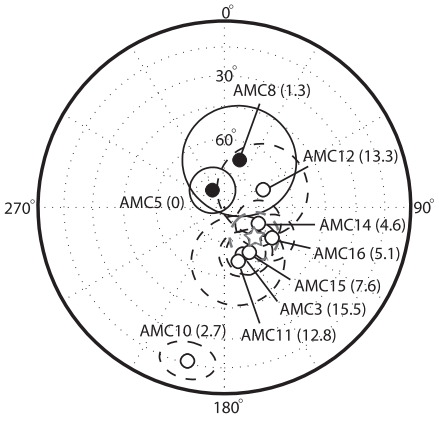

Fig. 2. Fusion-crust baked contact test on Angra dos Reis parent sample AMNH. HC magnetization directions of mutually oriented subsamples ranging from the fusion-crusted exterior to the interior are shown and plotted on an equal-area projection. Closed and open symbols represent projections of vector directions onto the lower and upper hemisphere, respectively. Ellipses give estimated orientation uncertainty (either MAD of least-squares fit or estimated sample positioning uncertainty, whichever is larger). Distance from fusion crust in millimeters is listed next to each sample. Only sample AMC5 contains fusion crust. The seven remaining samples are from the interior, with AMC8 and AMC10 apparently baked by atmospheric passage. Fisher mean direction (gray star) and associated 95% uncertainty confidence estimate (α_{95} = 10.7°) are shown for interior subsamples. The shallow depth of divergent magnetization directions (<3 mm) and the fact that measured samples have NRM/IRM < 1% throughout their full coercivity range indicate that the exterior has been thermally remagnetized by atmospheric passage rather than isothermally remagnetized by a magnet.

Three angrites record magnetic fields on the order of 10 μT on the APB extending from at least 4564.4 ± 0.1 (Pb/Pb age of the oldest angrite, D'Orbigny) to ≥4557.7 ± 0.1 Ma (Pb/Pb age of the youngest studied angrite, Angra dos Reis) (Fig. 3). Our fusion-crust baked contact test on Angra dos Reis and unidirectional magnetization trending to the origin observed in the interiors of Angra dos Reis and D'Orbigny (with Angra dos Reis having an especially low-noise signal) are collectively strongly indicative of primary thermoremanence. The implied paleointensities are ~20% of Earth's field today and far larger than that of the galactic field, solar wind, Mercury's present surface field, and the expected time-averaged fields of the T Tauri Sun outside 0.2 astronomical units (AUs) (Fig. 3). Angrite HC magnetization is highly unlikely to be the product of nebular lightning (*21*), which cannot produce the observed low NRM/IRM values. On the other hand, the paleointensities are within the range expected for the disk dynamo excited by magnetorotational instabilities (*22*), T Tauri flares at ~0.2 AUs, magnetic fields generated by large impacts (*2*), strong crustal ferromagnetic anomalies, and a core dynamo. However, our data indicate that the paleofields on the APB lasted for at least 10 My after CAIs, beyond the likely lifetime of a circumstellar disk dynamo (*23*). The absence of shock textures in angrites means that it is highly unlikely that the HC magnetization, which is blocked to coercivities >290 mT in Angra dos Reis, can be a shock remanence created in an impact-generated field (*24*). Additionally, the slow cooling rates of the coarse-grained angrites like Angra dos Reis (*25*, *26*) mean that they would have acquired their thermoremanence over a period of thousands to millions of years, far longer than the expected lifetime of any impact-generated fields [which last just ~1 day, even for basin-scale impacts on a Moon-sized body (*27*)] or T Tauri flares [lifetimes of several hours (*28*)]. Such slow cooling rates also make it highly unlikely that these angrites could have been magnetized by the spatially complex fields expected from magnetorotational instabilities while situated on the translating, spinning APB. Crustal field sources could potentially account for angrite magnetization, but such strong crustal fields would probably demand a core dynamo for their formation.

This reasoning implies that the source of these fields was internal, most likely a convecting metallic core and dynamo. Angrites contain geochemical evidence for the formation of an Fe-Ni core with a mass ~8 to 60% of the APB (*7*, *29*) by 4 My after CAIs (*4*, *30*), possibly coincident with

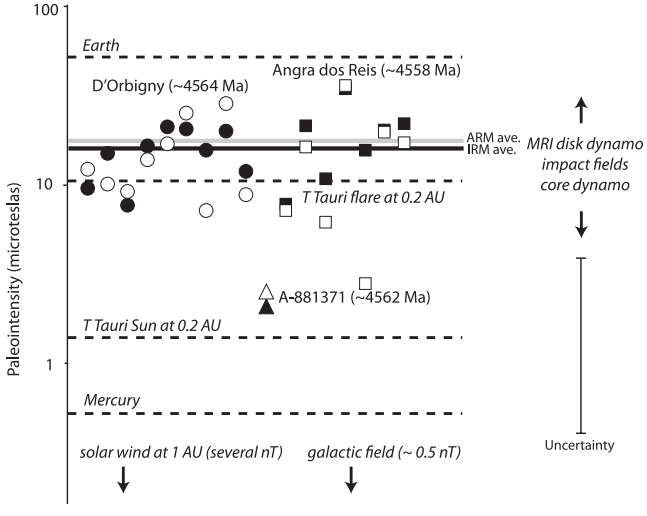

Fig. 3. Summary of paleointensity estimates for angrites. Each point is derived from the HC magnetization in a single subsample. Circles, D'Orbigny; triangles, A-881371; squares, Angra dos Reis (with approximate magnetization age labeled next to each meteorite). Solid symbols, IRM method; open symbols, ARM method using 50-μT bias field. Mean paleointensities from IRM and ARM methods are given by thick black and gray lines. For comparison, the surface fields of Earth and Mercury, the solar wind field at Earth's orbit (1 AU from the sun), the galactic field, and the inferred paleofields of the typical T Tauri sun and short-lived flares at 0.2 AUs are also shown. A magnetorotational instability (MRI) protoplanetary disk dynamo, impact plasma-generated fields, and core dynamos can produce paleointensities over a wide range of values, including values consistent with angrites. An estimate of the uncertainty range for an individual angrite paleointensity datum (primarily because of uncertainty in the ratio of ARM and IRM to thermoremanence) is shown at right.

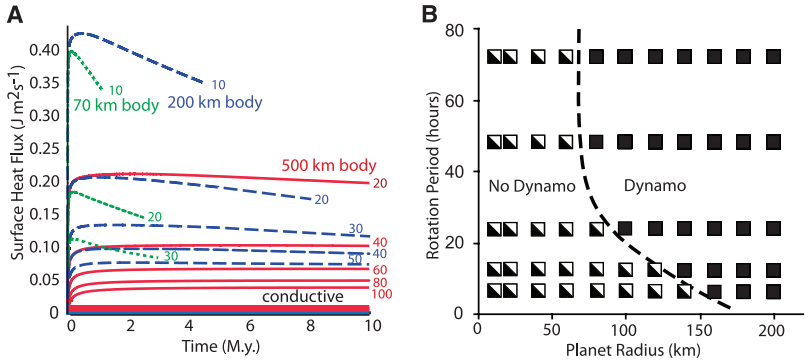

Fig. 4. Theoretical constraints on the possibility of dynamo generation on an early planetesimal. (**A**) Calculated outward heat flux from the surface of a model early planetesimal. The body is assumed to have a convecting magma ocean overlying a liquid Fe-Ni core and to be losing heat radiatively to space through a stagnant, conducting crustal lid (see SOM). The estimated power per unit surface area as a function of time after formation of the magma ocean [which is estimated to occur one to several My after accretion, see (*32*)] is shown. Calculations were conducted for bodies of radius 500 km (solid red lines), 200 km (dashed blue lines), and 70 km (dotted green lines) and for a variety of crustal thicknesses (numbers give thickness in kilometers). The dashed curves are terminated at the time when the magma ocean temperature drops below 850°C. Bold lines (all nearly overlapping at the bottom) indicate estimated maximum surface heat flux corresponding to a solely conductive adiabatic core. (**B**) Estimated conditions under which a planetesimal could produce a magnetic field like that recorded by angrites as a function of rotation period and planet size. Solid black squares indicate a supercritical magnetic Reynolds number and a planet surface field ≥20 μT (see SOM). Squares with lower left half in black indicate a surface field ≥20 μT, but a subcritical magnetic Reynolds number. The dashed line indicates the approximate boundary of angrite-like dynamo conditions.

an early magma ocean (*31*). Numerical modeling indicates that planetesimals will achieve >50 weight % melting and probably produce magma oceans if they accrete within ~1.3 My of CAIs and have radii exceeding ~20 km (*32*). On such bodies, it is conceivable that a metallic core would form quickly, setting the stage for an early, short-lived dynamo. We conducted two simple analytic calculations to assess this possibility (see SOM). Following (*32*), we assumed the core and silicate mantle of the body were initially molten and convecting beneath a solid conductive outer crust as a result of early internal heating by ^{26}Al decay. We found that for bodies with radii of 70 to 500 km and a wide range of crustal thicknesses, the heat flux out of the core is superadiabatic, a likely requirement for dynamo production (*33*) for periods lasting for several to several tens of million years after the end of major ^{26}Al heating (Fig. 4A). The main factor that terminates this early phase of superadiabatic heat flow is the progressive crystallization of the magma ocean: When the ocean temperature reaches ~850°C, we estimate that the ratio of crystals to liquid will be sufficiently high that convection will cease.

Second, we investigated the possibility that such bodies could produce a self-sustaining core dynamo and surface magnetic fields like that recorded in angrites (see SOM). Using various estimates of core convective velocities based on different scaling laws, we found that bodies with radii exceeding ~80 km and a wide range of spin rates, internal density distributions, and core sizes [including possibly ancient Mercury (*34*)] can have supercritical magnetic Reynolds numbers and produce surface fields exceeding 20 μT (Fig. 4B). These calculations are illustrative of the feasibility (perhaps even inevitability) of early planetesimal dynamos.

Magnetization in angrites pre-dates that in howardite-eucrite-diogenite meteorites (thought to be from the asteroid Vesta) (*35*) and lunar (*36*), martian (*37*), and terrestrial rocks (*38*) by ~100 to 1000 My. Our paleomagnetic data are a unique geophysical contribution to a growing body of geochemical evidence indicating that planets and large planetesimals formed metallic cores within just a few million years after CAIs. If the APB is representative of these quickly formed bodies, short-lived planetesimal core dynamos may have been a widespread process in the early solar system.

References and Notes

1. Previous paleomagnetic studies have been conducted on five small-body basaltic achondrite groups: the howardite-eucrite-diogenites, Ibitira, ureilites, mesosiderite clasts, and aubrites.
2. D. A. Crawford, P. H. Schultz, *Int. J. Impact Eng.* **23**, 169 (1999).
3. Y. Amelin, *Geochim. Cosmochim. Acta* **72**, 221 (2008).
4. A. Markowski *et al.*, *Earth Planet. Sci. Lett.* **262**, 214 (2007).
5. R. E. Zartman, E. Jagoutz, S. A. Bowring, *Lunar Planet. Sci.* **XXXVIII**, 1580 (abstr.) (2006).
6. H. Busemann, S. Lorenzetti, O. Eugster, *Geochim. Cosmochim. Acta* **70**, 5403 (2006).
7. G. Kurat *et al.*, *Geochim. Cosmochim. Acta* **68**, 1901 (2004).
8. M. Prinz *et al.*, *Earth Planet. Sci. Lett.* **35**, 317 (1977).
9. D. W. Mittlefehldt, T. J. McCoy, C. A. Goodrich, A. Kracher, in *Planetary Materials*, J. J. Papike, Ed. (Mineralogical Society of America, Washington, DC, 1998), pp. 4-1–4-195.
10. G. McKay, D. Lindstrom, S.-R. Yang, J. Wagstaff, *Lunar Planet. Sci.* **XIX**, 762 (1988).
11. S. M. Kuehner *et al.*, *Lunar Planet. Sci.* **XXXVII**, 1344 (abstr.) (2006).
12. K. Yanai, *Proc. NIPR Symp. Antarc. Geosci.* **7**, 30 (1994).
13. P. H. Warren, A. M. Davis, *Antarct. Meteorites* **XX**, 257 (1995).
14. D. W. Mittlefehldt, in vol. 1 of *Treatise on Geochemistry*, H. D. Holland, K. K. Turekian, Eds. (Elsevier, Amsterdam, 2007), pp. 1–40.
15. D. J. Dunlop, *J. Geophys. Res.* **111**, B12S02 (2006).
16. O. A. Derby, *Revista do Observatorio* **3**, 33 (1888).
17. L. Spivak-Birndorf, M. Wadhwa, P. E. Janney, *68th Annual Meteoritical Society Meeting*, abstract 509 (2005).
18. As discussed in the SOM, we conducted ARM and IRM paleointensity experiments but did not conduct thermal paleointensity experiments. Although thermal paleointensities are in principle the most accurate, our thermomagnetic data (fig. S9) suggest that the meteorites would probably alter during such experiments, which would compromise their efficacy while destroying the samples.
19. T. Mikouchi, M. Miyamoto, G. McKay, L. Le, *64th Annual Meteoritical Society Meeting*, abstract 5344 (2001).
20. These fast cooling rates mean that the Pb/Pb ages should provide a good estimate of the time by which the meteorites first cooled to ambient temperatures. Fast cooling also implies that the meteorites should be unaffected by low-temperature metal recrystallization that can complicate slower-cooled samples.
21. S. J. Desch, J. N. Cuzzi, *Icarus* **143**, 87 (2000).
22. S. A. Balbus, *Annu. Rev. Astron. Astrophys.* **41**, 555 (2003).
23. S. S. Russell *et al.*, in *Meteorites and the Early Solar System II*, D. S. Lauretta, H. Y. McSween, Eds. (Univ. of Arizona, Tucson, AZ, 2006), pp. 233–251.
24. J. Gattacceca *et al.*, *Phys. Earth Planet. Inter.* **166**, 1 (2008).
25. D. Störzer, P. Pellas, *Earth Planet. Sci. Lett.* **35**, 285 (1977).
26. G. McKay, T. Ogawa, M. Miyamoto, H. Takeda, *Lunar Planet. Sci.* **XXIV**, 967 (1993).
27. L. L. Hood, N. A. Artemieva, *Icarus* **193**, 485 (2008).
28. J.-P. Vallée, *N. Astron. Rev.* **47**, 85 (2003).
29. K. Righter, *Lunar Planet. Sci.* **XXXIX**, 1936 (abstr.) (2008).
30. A. Shukolyukov, G. W. Lugmair, *Lunar Planet. Sci.* **XXXVIII**, 1423 (abstr.) (2007).
31. R. C. Greenwood, I. A. Franchi, A. Jambon, P. C. Buchanan, *Nature* **435**, 916 (2005).
32. P. J. Hevey, I. S. Sanders, *Meteorit. Planet. Sci.* **41**, 95 (2006).
33. D. J. Stevenson, *Earth Planet. Sci. Lett.* **208**, 1 (2003).
34. S. Stanley, J. Bloxham, W. E. Hutchison, M. T. Zuber, *Earth Planet. Sci. Lett.* **234**, 27 (2005).
35. D. W. Collinson, S. J. Morden, *Earth Planet. Sci. Lett.* **126**, 421 (1994).
36. I. Garrick-Bethell, B. P. Weiss, *Lunar Planet. Sci. Conf.* **XXXVIII**, 2405 (abstr.) (2007).
37. B. P. Weiss *et al.*, *Earth Planet. Sci. Lett.* **201**, 449 (2002).
38. C. J. Hale, *Earth Planet. Sci. Lett.* **86**, 354 (1987).

39. We thank T. Irving for introducing us to angrites and G. Hupé for providing NWA 2999, NWA 4801, and NWA 4931; E. Jagoutz and La Memoire de la Terre for D'Orbigny; D. Ebel and M. Zucolotto for Angra dos Reis; and the National Institute of Polar Research in Japan for A-881371. L. Bei and C. Ross gave us access to their vibrating sample magnetometer for rock magnetic analyses, N. Chatterjee assisted with electron microscopy, and D. Shim assisted with Raman spectroscopy. We also thank T. Bosak and M. Zuber for advice, M. Varela for information on the handling history of D'Orbigny, and K. Willis for administrative help. This study relied on automated paleomagnetic technology shared by J. Kirschvink. This work was partially supported by the NSF Instrumentation and Facilities Program (to B.P.W.).

Supporting Online Material

www.sciencemag.org/cgi/content/full/322/5902/713/DC1
SOM Text
Figs. S1 to S12
Tables S1 to S5
References

27 June 2008; accepted 25 September 2008
10.1126/science.1162459

Supporting Online Material for

Magnetism on the Angrite Parent Body and the Early Differentiation of Planetesimals

Benjamin P. Weiss,* James S. Berdahl, Linda Elkins-Tanton, Sabine Stanley, Eduardo A. Lima, Laurent Carporzen

*To whom correspondence should be addressed. E-mail: bpweiss@mit.edu

Published 31 October 2008, *Science* **322**, 713 (2008)
DOI: 10.1126/science.1162459

This PDF file includes:

Supporting Online Material

Weiss, B. P. *et al.* (2008) Magnetism on the Angrite Parent Body and the Early Differentiation of Planetesimals, *Science*

1.0. Introduction

Measurements of natural remanent magnetization (NRM) were taken in the MIT Paleomagnetism Laboratory with a 2G Enterprises Superconducting Rock Magnetometer 755 housed inside a magnetically shielded room (DC field < 150 nT). Nearly all sample handling was conducted inside a class 10,000 clean laboratory within this shielded room. Chips were subsampled using nonmagnetic tools and a precision wafering saw. Sample moments were measured prior to and following subsampling and a comparison of the vector sum of subsamples with the parent moment demonstrated that sawing and chipping did not remagnetize the samples.

Because of the great value and scarcity of angrites, we made the fundamental decision to conduct nondestructive magnetic analyses of our samples. This allowed us to conduct a large range of rock magnetic analyses *on the very same samples* for which we had measured and demagnetized NRM. With the exception of a small number of thermomagnetic analyses, samples were demagnetized and remagnetized using alternating field (AF) and isothermal methods. This decision proved to have the unexpected but critical advantage over thermal demagnetization methods of allowing us to identify and usually completely remove isothermal remanent magnetization (IRM) from collectors' magnets that commonly overprints the exteriors of angrites and other meteorites (*S1-3*). The major disadvantages of not doing thermal demagnetization are the inability to assess the blocking temperature distribution of NRM and to conduct Thellier-Thellier paleointensity analyses.

Three axis AF demagnetization and rock magnetic remanence experiments were conducted using an automated sample handling system integrated with the magnetometer (*S4*). At intervals of 10 mT, selected samples from each meteorite were subjected to uniaxial AF demagnetization in each of the three orthogonal axes to test whether the NRM vector was being affected by spurious gyromagnetic remanent magnetization (GRM) and/or field-impressed anisotropy (*S5-9*). All samples were AF demagnetized until either their moments were dominated by spurious anhysteretic remanent magnetization (ARM) induced by our AF system [e.g., (*S10-14*)] or, in several cases by GRM and/or field impressed anisotropy. Following demagnetization of NRM, paleointensities were estimated using AF methods and a series of rock magnetic experiments were conducted to assess the fidelity of their magnetic records and determine the ferromagnetic mineralogy. Selected samples were also subjected to magnetic viscosity, hysteresis, and low-temperature cycling analyses. Finally, all samples were analyzed using progressive isothermal remanent magnetization (IRM) and ARM acquisition and AF demagnetization of IRM and ARM. We discuss each of these experiments in turn. We then describe our theoretical investigation into the feasibility of angrite-like paleofield generation by a core dynamo on an early planetesimal. We end by

discussing the implications of our paleomagnetic measurements and dynamo modeling for the hypothesis that Mercury is the angrite parent body.

2.0. Data on ferromagnetic mineralogy and crystal size

2.1. Hysteresis data. Hysteresis loops at room temperature on selected samples from each meteorite were measured in order to constrain the mineralogy, domain size and saturation field (Fig S4). Measurements were acquired with a Digital Measurement Systems vibrating sample magnetometer (VSM) in the laboratory of C. Ross at MIT. The high-field slope of each hysteresis loop was used to estimate the contribution of paramagnetic minerals. This contribution has been subtracted from the loops shown in Fig S4. Following Dunlop (*S15*), D'Orbigny, A-881371 and one of the Angra dos Reis samples (M2) have ratios of saturation remanence to saturation magnetization (M_{rs}/M_s) and coercivity of remanence to coercivity (H_{cr}/H_c) that fall along the single domain-multidomain mixing line (Table S1) [although we note that Dunlop's calculations (*S15*) are strictly only valid for magnetite, whereas as described below Angra dos Reis clearly contains a second ferromagnetic mineral in addition to magnetite]. The other sample of Angra dos Reis (3S1) is significantly displaced from the single domain-multidomain line toward the single domain-superparamagnetic mixing line.

2.2. Anhysteretic remanent magnetization (ARM) and isothermal remanent magnetization (IRM) experiments. After the completion of AF demagnetization of NRM, samples were given stepwise ARM in increasing DC bias fields from 0.5 to 2 mT in a peak AC field of 200 mT. These data can be used to infer the degree of magnetostatic interactions in the sample (*S16*). Following this, the ARM was then stepwise AF demagnetized. Then, the samples were given an IRM with a DC field of 200 mT that was also subsequently stepwise AF demagnetized. The IRM acquisition and AF demagnetization of IRM data are indicators of the coercivity spectrum of the sample. Comparison of the AF demagnetization of ARM and IRM constitutes the Lowrie-Fuller test, an indicator of grain size and stress state (*S17, 18*).

The results of these experiments are summarized in Table S2. ARM acquisition data indicate that all the meteorites have highly interacting grains (Fig. S5). The slow-cooled angrite Angra dos Reis has a Lowrie-Fuller test with low-field type (L-type; ARM more stable than IRM) behavior character, whereas the "quenched" angrites D'Orbigny and A-881371 exhibit behavior intermediate between L-type and high-field type (H-type, IRM more stable than ARM) (Fig. S6). This difference between slowly-cooled and quenched angrites likely is not a result of differences in crystal size because our hysteresis loops indicate that the quenched angrites are actually finer grained than the slowly cooled angrites (as expected from petrographic observations). Rather, the difference between these two classes of angrites may be reflective of differences in either internal stress state or ferromagnetic mineralogy.

With respect to mineralogy, IRM acquisition and demagnetization data (Fig. S7) and associated S ratios (*S19, 20*) and coercivity of remanence values (Table S2) indicate that unlike the other two angrites, Angra dos Reis shows a clearly bimodal coercivity spectrum reflective of two main ferromagnetic minerals, one with coercivities up to ~ 300 mT and a second, higher coercivity phase.

2.3. Low-temperature cycling. To search for low-temperature transitions diagnostic of some ferromagnetic minerals, low-temperature magnetic data were acquired for each meteorite (Fig S8). Samples were first exposed to a saturating (4 T) field at room temperature and then their moments were continuously measured while the samples were cycled in a weak (< ~200 μT, the minimum field in our MPMS) field down to 10 K and back up to room temperature. All the angrites exhibited a low-temperature transition at ~45 K below which the spontaneous magnetization of the samples increased dramatically. Given the major phases reported for these angrites, this likely reflects the ordering of the low-Ti spinel phase whose homogenous mean composition ($hercynite_{38\text{-}50\%}$-$spinel_{26\text{-}50\%}$-$chromite_{4\text{-}9\%}$-$magnesiochromite_{5\text{-}7\%}$-$magnetite_{2\text{-}7\%}$-$ulvöspinel_{0\text{-}4\%}$ for D'Orbigny) has its Curie point near this temperature (*S21-25*).

2.4. Thermomagnetic data. Following the completion of all other rock magnetic experiments, thermomagnetic data (saturation remanent magnetization as a function of temperature) were measured for several samples to determine Curie points and search for any magnetic transitions potentially diagnostic of the ferromagnetic mineralogy (Fig. S9). These measurements were acquired with the VSM in the Ross laboratory at MIT in an argon atmosphere from room temperature up to 700°C (maximum limit of instrument). Room-temperature hysteresis loops were taken before and after the thermomagnetic measurements to assess whether the samples were altered during heating. The results suggest that the dominant ferromagnetic mineral in D'Orbigny has a Curie point near 575°C. Angra dos Reis appears to contain a major phase with a Curie point of 550°C, Both of these results, particularly those for Angra dos Reis, are somewhat uncertain due to irreversibility (sample alteration) observed during the experiment.

2.5. The ferromagnetic mineralogy of angrites. These two Curie temperatures are very similar and are characteristic of one or more of several candidate minerals: titanomagnetite, taenite, tetrataenite, titanohematite, or titanomaghemite. Ni-rich metal has only been reported for D'Orbigny (*S26*), so tetrataenite and taenite can immediately be discounted for the other angrites. Taenite (*S27, 28*) can be additionally discounted for D'Orbigny (as well as for the other angrites) because it almost always has multidomain properties with coercivities far below that observed for these meteorites (Fig. S4, Table S1). Tetrataenite (*S27, 28*) can also be discounted for D'Orbigny and the other angrites for further reasons: the post-heating hysteresis loops do not exhibit the characteristic drop in M_{rs}, H_{cr} and H_c after heating, the thermomagnetic curves are not blocky, and finally the angrites have cooling rates well exceeding the 1-100°C $m.y.^{-1}$ required for the formation of this mineral (*S29*). Titanohematite and titanomaghemite are also highly unlikely for two reasons: optical and electron microscopy studies of angrites have never identified these phases (they are typically terrestrial weathering minerals while microscopy data indicate that none of the four angrites considered here is significantly weathered) and titanomaghemite almost always breaks down well before its Curie point. Although Angra dos Reis exhibits similar irreversibility, this is almost certainly due the high abundance of troilite (*S30-32*) in this meteorite (*S33*).

This leaves magnetite as the only likely explanation. Indeed, our IRM-acquisition and hysteresis data are all consistent with its presence. Primary (preterrestrial) low-Ti magnetite has been previously reported for A-881371. Furthermore, our electron

microscopy investigation (Section 3.0, Fig. S10) has now also identified low-Ti magnetite in D'Orbigny. The latter should have a Neel temperature near 550°C, slightly lower than that observed in the thermomagnetic data (Fig. S9).

In addition to low-Ti magnetite, at least three other accessory ferromagnetic phases must be present in angrites. D'Orbigny exhibits a secondary Curie point at ~150°C (Fig. S9), probably indicative of the abundant high-Ti magnetite phase reported in this and nearly all other angrites (although the typically reported composition, magnetite$_{0.17\text{-}0.21}$-ulvöspinel$_{0.71\text{-}0.77}$, should only have a Neel point of up to ~40°C) (*S26, 33-39*). The bimodal IRM-acquisition curves (Fig. S7) and S ratios well below unity (Table S2) of Angra dos Reis indicate an additional high-coercivity phase; given the known phases in this meteorite, this is likely either kamacite or pyrrhotite. Both phases have been previously reported in angrites (*S26, 33, 40, 41*). Although no 34 K transition characteristic of monoclinic pyrrhotite is visible in our low-temperature cycling data (Fig. S8), it is possible that this transition could have been suppressed by impurities [although the effect of impurities on the intensity of the transition is unknown, monoclinic pyrrhotite has been reported for Martian meteorite ALH 84001 (*S42*) despite the lack of a 34 K transition for that meteorite (*S43*)]. It is highly unlikely that angrites contain ferromagnetic hexagonal pyrrhotite (*S44*) because even the fasted cooled "quenched" angrite D'Orbigny cooled at a rate two orders of magnitude slower (*S45*) than that required to produce this metastable phase (*S46*).

3.0. Electron microscopy data. Of the four angrites studied here, one is a quickly recovered fall (Angra dos Reis), one is from Antarctica (A-881371), and one was found in a field in Argentina. All three meteorites are extremely fresh. The first two contain primary metal, troilite, titanomagnetite, and magnetite (*S33, 39, 47*), and therefore it is highly unlikely that their ferromagnetic mineralogy has an origin by terrestrial weathering. Published images of D'Orbigny also indicate it is very fresh and it is known to contain titanomagnetite as well as magnetite of unspecified composition (*S26, 36, 48-50*). To determine the exact composition of this magnetite and characterize its textural relationships with surrounding igneous phases, we conducted backscatter electron microscopy imaging and quantitative wavelength dispersive spectroscopy analyses on a polished thick section of D'Orbigny (sample FB14). We identified a wide range of phases with compositions ranging from about $Fe_{2.0}Ti_{0.3}Al_{0.7}O_4$ to near end member magnetite ($Fe_{2.9}Z_{0.1}O_4$ for various impurities, Z) (Fig. S10). These crystals exhibited primary igneous textural relationships with surrounding phases. All sulfide grains imaged showed no weathering or alteration and no mantling, veins, or common weathering minerals like goethite, maghemite, and hematite were detected anywhere in our section. Note that these images only resolved multidomain grains and not the fine grained carriers that dominate the remanence as implied by the hysteresis data (Section 2.1).

4.0. Magnetic viscosity experiments

Néel theory calculations for magnetite, pyrrhotite, and kamacite (*S51-54*) indicate that magnetization carried by grains with 1-h blocking temperatures above ~150-250°C are stable during exposure to room temperatures over the history of the solar system, indicating that the magnetization in angrites was probably slightly viscously

demagnetized before arriving on Earth. Following landing, many of these demagnetized grains may then have acquired a viscous remanent magnetization (VRM) in the Earth's field. Angra dos Reis and A-881371 landed on the Earth in 1869 (*S55*) and at <60 ka (*S56*), respectively, while no terrestrial age has been reported for D'Orbigny. It is important to (*i*) establish that the HC magnetization observed in angrites is not entirely a terrestrial VRM and (*ii*) assess whether the nearly ubiquitous low coercivity (non-IRM) overprints observed in our samples are a terrestrial VRM (as opposed to preterrestrially acquired overprints).

For Angra dos Reis, our fusion crust baked contact test alone essentially rules out terrestrial VRM (as well as any other magnetization acquired on Earth) as the main source of the meteorite's HC magnetization. For the other two meteorites, we can examine two additional criteria: stability of the various NRM components and laboratory VRM acquisition rate. In the absence of thermal demagnetization data, probably the best way to assess the contribution of VRM is by examination of the coercivity range of the observed LC components (identified by directional changes in the NRM). The coercivity range depends on VRM acquisition time, grain coercivity and volume distribution, mineralogy, and temperature history and is therefore difficult to predict. Previous studies of magnetite-bearing basalts with VRM acquired at ambient surface temperatures over periods ranging from 1 month to ~50 ky have found that VRM can be mostly erased by AF fields of ~5-40 mT [see, for instance, (*S57-60*)]. For comparison, the LC components in A-881371 sample ,63 and D'Orbigny sample F6 (neither of which have IRM-overprints from magnets as indicated by our paleointensity data and/or directional homogeneity tests), are essentially entirely erased by 8.7 mT and 6.6 mT, respectively. Many Angra dos Reis AMNH samples exhibit LC components blocked to between 5-15 mT. An exception is sample AMC16, which exhibited no obvious LC component during AF demagnetization (main text Fig. 1C); however, our paleointensity experiments (Fig. S2C,D) suggest the sample is unmagnetized up to ~11 mT, probably due to relaxation in our shielded room over the last 6 months. The HC components observed in A-881371 sample ,63, D'Orbigny sample F6, and Angra dos Reis sample AMC16 extend to at least 150 mT, 150 mT, and 290 mT (see Fig. 1C for AMC16), respectively. This suggests that (a) the LC components in these meteorites are likely VRM acquired on Earth and (b) the HC components are unlikely to be terrestrial VRMs.

To further test this conclusion, we measured the acquisition rate of VRM in our laboratory for selected subsamples of each meteorite. The samples were exposed to the Earth's local field (~50 μT) for a period ranging from between several days to several weeks. The samples were then brought into the shielded room and their remanence measured repeatedly over a time period up to that spent outside the room. In many cases, negligible VRM was acquired during the experiments, while for the other samples detectable but only moderate VRM was acquired.

An example of the latter behavior is that observed for Angra dos Reis sample M7 (Fig. S11A,B). The VRM acquired by M7 during 14.6 d of exposure to the Earth's field was equal to approximately 10% of the estimated original NRM upon landing on Earth in 1869 (inferred from a linear extrapolation of the HC paleointensity data to zero ARM gained). Following an initial plateau, the VRM was observed to decay at a rate roughly proportional to the logarithm of time (Fig. S11A), $S_d = dM/d(\log t) = 8.3\times10^{-12}$ Am^2 (log s)$^{-1}$. About 90% of the VRM gained during the time interval outside the shielded room

had decayed after the same time interval had elapsed inside the shielded room, suggesting that the rate of acquisition rate of VRM, S_a is approximately equal to S_d [previous investigators (*S61-65*) have found that S_a and S_d usually differ no more than a factor of 2]. Assuming that same logarithmic rate with time with $S_a = S_d$ over the entire 139 y residency of Angra dos Reis on Earth [and noting the considerable uncertainties associated with such an extrapolation (*S62, 66*)], we estimate that a VRM equal to about 25% of the preterrestrial NRM of this sample was acquired on Earth.

Although this particular sample exhibited nearly linear VRM decay with log(time) in the measured time interval, other samples exhibited non-logarithmic decay rates (Fig. S11C,D). Such behavior has been observed by nearly all previous investigators of VRM, and underscores the uncertainties associated with extrapolations of data acquired on laboratory timescales. The best that we can say is that linear extrapolations of the highest-time data in our experiments for our angrite samples leads to the same basic conclusion as that derived from sample Angra dos Reis sample M7: VRM acquired on Earth is unlikely to entirely account for the intensity of the HC components observed in angrites. The sample most dominated by VRM is A-881371, whose LC component represents about 71% of its estimated preterrestrial NRM (again inferred from a linear extrapolation of the HC paleointensity data to zero ARM gained). Linear extrapolation of the high-time tail of our VRM experiments (Fig. S11C) to the meteorite's terrestrial age predicts a VRM intensity about a factor of 2 lower than the actually observed LC component. Given the uncertainties involved in this exercise, we consider this reasonably good agreement.

5.0. Paleointensity experiments

5.1. Paleointensity protocol. Nearly every sample was subjected to each of four AF paleointensity experiments. The goal of these experiments was to obtain *nondestructive*, *order-of-magnitude* estimates of the intensity of the magnetizing paleofield on the angrite parent body. We note that although such uncertainties are high by terrestrial standards, the questions being asked in extraterrestrial and terrestrial paleomagnetism are different: with angrites, we are trying to distinguish between field sources that vary in intensity by many orders of magnitude (main text Fig. 3) rather than trying to study secular variation, relationships between reversal frequency and paleointensity, and other time-variable processes that require much better accuracy.

Three kinds of our paleointensity experiments used ARM as a normalizing quantity in three different DC bias fields, while the fourth experiment used saturation IRM as the normalizing quantity. The artificial ARM and IRM were stepwise AF demagnetized using the same steps as used to demagnetize the NRM, permitting us to compute NRM/ARM and NRM/IRM for each coercivity bin and therefore for each NRM component. Our paleointensity methods are multicomponent techniques: our IRM method is in essence the same as the REM' and REM(AF) techniques (*S1, 67*), while our other paleointensity technique is philosophically equivalent to REM' except that ARM is used as the normalizer in place of IRM.

It has been demonstrated from studies of a wide variety of terrestrial, and extraterrestrial minerals and their synthetic analogs that the ratio of a thermoremanent NRM to the saturation IRM is roughly proportional to the intensity of the paleofield which produced the NRM (*S1, 68-74*). Samples containing approximately equant crystal

shapes will have NRM/IRM ~ several % for a TRM component produced in Earth's field (~50 μT), although extreme acicular shape and size distributions can have NRM/IRM that is 50 times higher than that of equant grains (*S68, 75*). For such samples, the paleointensity estimate from this technique has an uncertainty of a factor of ~10, with the chief sources of error being the dependence of TRM intensity on the unknown grain volume and microscopic coercivity distribution (*S76, 77*).

Analogously to the IRM method, the ratio of thermoremanent NRM to ARM (sometimes called *f'*) is also roughly proportional to the NRM paleointensity (*S78-83*); this paleointensity estimate will be most accurate when the ARM bias field is close to that which produced the NRM (*S84*). Samples containing magnetite with diameters greater than ~0.05 μm or less than 0.5 μm will have NRM/ARM(50 μT bias) ~ 2 for a TRM component produced in a 50 μT paleofield. The ARM paleointensity technique also has an uncertainty of a factor of ~10, with the chief uncertainty due to the dependence of ARM/TRM on the unknown grain volume distribution (*S85-89*).

For all but two subsamples, we first conducted three paleointensity experiments in which ARM was acquired in increasing AF fields for constant bias fields of 50, 200, and then 600 μT. These samples were then given a saturation IRM that was then AF demagnetized. Paleointensity estimates (Table S3) were obtained from plots of NRM lost versus ARM gained [similar to the Stephenson method (*S78*)] and NRM lost versus IRM lost [essentially the REM' method of Gattacceca and Rochette (*S1*) but using the visualization method of Stephenson (*S78*) to reduce the effects of spurious ARM noise from our AF system]. NRM lost was computed using vector subtraction for each component. HC components were identified directionally in Zijderveld diagrams and then paleointensity values were derived from linear regressions of the equivalent HC data in the paleointensity plots. For example, two components—LC (blue symbols) and HC (red symbols)—were observed in D'Orbigny sample F1 (Fig. 1A) while one component was observed in Angra dos Reis sample AMC16 (Fig. 1C). In the paleointensity experiment for F1 (Fig. S2A,B), NRM lost values up to AF 6.6 mT were computed by vector subtraction from the NRM, while NRM lost values above AF 6.6 mT were computed by vector subtraction from the AF 6.6 mT step. For AMC16 (Fig. S2C,D), NRM lost values up to AF 18 mT were computed by vector subtraction from the NRM, while NRM lost values above 18 mT were computed by vector subtraction from the AF 18 mT step.

Because all samples were in the pseudo single domain size range (Section 2.0), we calculated the IRM and ARM paleointensities using the following formulas and calibration factors:

$$\text{ARM paleointensity in microteslas} = (\Delta\text{NRM}/\Delta\text{ARM})/2 \times (\text{bias field in microteslas})$$
$$\text{IRM paleointensity in microteslas} = \Delta\text{NRM}/\Delta\text{IRM} \times 3000,$$

where ΔNRM, ΔARM, ΔIRM are, respectively, the vector-subtracted gain or loss of NRM, ARM, and IRM as derived from least squares fits to the paleointensity plots in the AF range for the HC component. The IRM used for these paleointensity experiments was usually acquired in a 1 T field (near saturation), whereas the ARM peak field was usually 200 mT.

The magnitude of the NRM of two subsamples did not substantially decay in intensity during AF demagnetization after removal of LC magnetization (Table S3). Although positive slopes are observed for these samples in both the ARM and IRM paleointensity plots, these data may be contaminated by spurious AF-related noise. We therefore calculated the paleointensity values for these samples by a second method in which the NRM remaining after removal of the LC component is divided by the ARM and IRM remaining removal of the LC component. This method, known as the residual REM method for IRM paleointensities (*S1, 71*), makes the implicit assumption that there is a single remaining HC component.

5.2. Uncertainties. There are two aspects in which our paleointensities are uncertain. The first and most important is the unknown efficiency of NRM relative to ARM and IRM discussed above. The second is that our estimates of NRM/ARM and NRM/IRM from our linear regressions are limited by AF-related spurious ARM (see, for instance Fig. S3). We estimated the latter uncertainty by computing 95% confidence intervals for the slope fits using a two-tailed Student's *t*-test (*S90*) (Table S3).

Because all samples in Table S3 were found to have paleointensities of a few tens of μT, the ARM paleointensities obtained using the 50 μT bias field should have mean values closer to the true paleointensity than those from the 200 and 600 μT ARM experiments. However, the 50 μT paleointensities have the highest uncertainty due to the weakness of the bias field and therefore the greater influence of spurious AF-related ARM noise.

Remanence anisotropy is another possible error source. However, we found that all three meteorites have low remanence anisotropy on the scale of our subsamples (tens of mg). For instance, for Angra dos Reis sample M2, ARM (200 mT AC field, 2 mT DC bias) and IRM 164 mT applied in the three orthogonal directions varied in magnitude by a maximum of 4% and 1%, respectively, and deviated from the applied field direction by a maximum of 8° and 6°, respectively. For D'Orbigny sample F1, ARM (200 mT AC field, 2 mT DC bias) and IRM 164 mT applied in the three directions varied in magnitude by a maximum of 5% and 7%, respectively, and deviated from the applied field direction by a maximum of 2° and 1°, respectively. For A-881371 sample ,63, ARM (200 mT AC field, 0.2 mT DC bias) and IRM 200 mT applied in the three directions varied in magnitude by a maximum of 15% and 0.6%, respectively, and deviated from the applied field direction by a maximum of 3° and 2°, respectively. Therefore, we did not make any anisotropy corrections (*S91*) in computing the paleointensities reported in Table S3.

For two samples, the IRM paleointensity experiment was conducted before the ARM experiments; because we could not fully demagnetize the saturation IRM prior to beginning the ARM experiments, this resulted in high ARM paleointensity uncertainties for these two samples.

5.3. Magnet contamination tests. As discussed previously, some of our subsamples have been partially overprinted by hand magnets. During AF demagnetization, we observed directional changes in the magnetization vector to origin-trending HC components that correlate with a distinct break in slope in ARM and IRM paleointensity plots, indicating that the LC components should not be contaminating our HC paleointensity estimates. To confirm this, for every sample we conducted magnetic contamination tests in which

samples were given a laboratory IRM in a field equal to that inferred to have created the LC magnet component measured during AF demagnetization of NRM. We then AF demagnetized the samples, and in all cases observed that the laboratory LC magnetization was completely removed at an AF level close to the applied field value.

We conducted additional experiments in which samples were given an ARM to yield an artificial HC paleointensity equal to the inferred natural thermoremanent HC paleointensity (assuming the ratio of thermoremanence to ARM is ~2 as discussed above). The samples were then overprinted with an approximately perpendicular IRM in a field equal to that inferred to have created the LC magnet component. We then AF demagnetized these samples and used these data to construct ARM and IRM paleointensity plots for this artificial magnetization. In all cases, a clear break in the direction of magnetization and slope in the paleointensity plot were observed near the applied DC field value. Paleointensities from the magnetization above this value agreed with the actual field intensity that created the artificial HC magnetization within the expected uncertainties. An example of such experiments is shown in Fig. S12.

6.0. Modeling early planetesimal dynamos

We have argued in the main text that the prolonged record of angrite magnetism (lasting at least 10 m.y. after solar system formation and at least 7 m.y. after the formation of the parent body) as well as the substantial angrite paleointensities (in some cases exceeding 20 μT) suggest that the magnetizing field was generated by an internal core dynamo. This proposal would be greatly strengthened if theoretical estimates confirmed that such an intense, ≥7 m.y. long dynamo is feasible on typical planetesimal objects. We addressed this question by examining whether (a) convection of a metallic liquid core could be initiated on the angrite parent body and how long this would last and (b) whether this core could produce surface magnetic fields exceeding 20 μT.

Our simplified approach was to consider the model bodies of Hevey and Sanders (*S92*), in which sufficiently large and early-formed planetesimals acquired global magma oceans due to radiogenic heating by ^{26}Al. Under these conditions, melting may have occurred from the interior outward, leaving a solid conductive lid overlying a magma ocean and a liquid metallic core. The quenched angrites may have originated as melts that erupted through the solid crust and solidified, thereby recording the field, while the slowly cooled angrites formed parts of the conductive lid that slowly cooled through their Curie temperatures. Because the magma ocean likely had high Rayleigh number and was vigorously convecting (*S93*), heat conduction through the crust should have ultimately limited heat flux out of the core.

6.1. Timing of core convection. A straightforward scenario leading to a core dynamo is one in which thermal convective motion of the conducting Fe-Ni liquid is driven by heat loss from the planet. For this to occur, the heat flux out of the core should at minimum exceed the heat flux that would be carried by conduction along a core adiabat (*S94*), $F_{cond} = k\alpha Tg/C_p = 4\pi G\rho rk\alpha T$, where k is thermal conductivity [taken conservatively to be 50 W m^{-1}K^{-1}, following (*S95*)], α is thermal expansivity [10^{-4} K^{-1} following (*S96*)], T is the temperature at the core-mantle boundary [~1273 K when the body is just at the solidus temperature (*S96*)], C_p is the heat capacity at constant pressure [800 J kg^{-1}K^{-1} for the core following (*S97*)], and $g = 4\pi G\rho r$ is the gravitational acceleration for gravitational

constant G, core density ρ, and core radius r. For 70 km, 200 km, and 500 km radius bodies with 10 km, 63 km and 350 km radius cores that are just cool enough to have a solid mantle, we find that $F_{cond} = 5.7\times10^{-4}$, 0.0034, and 0.0187 J $m^{-2}s^{-1}$, respectively. These are the estimated core heat fluxes that must be exceeded to produce a dynamo.

The next step is to determine if and when the cores of our model planetesimals have heat flows exceeding this criterion. We calculated heat conduction through the solid crustal lid with a one-dimensional model using the following expression for temperature controlled by conduction in a spherical shell:

$$T(t,r) = T(t-dt,r) + \kappa dt\left\{\frac{1}{r}dr\left[T(t-dt,r+dr) - T(t-dt,r-dr)\right]\right.$$
$$\left. + \frac{1}{dr^2}\left[T(t-dt,r - 2T(t-dt,r) + T(t-dt,r-dr)\right]\right\}$$

for time t and distance r from the center of the body. Because our calculations start at times ≥3 m.y. after CAIs, we have neglected radiogenic heating from ^{26}Al (which otherwise might blanket the core). We have also neglected any heating from ^{60}Fe because angrites apparently did not contain this short-lived isotope (*S98*) (which otherwise would enhance core convection). We used parameter values characteristic of asteroids with a range of different body and core sizes (Table S4). We assumed that the magma ocean under the lid begins at approximately the liquidus temperature for the estimated bulk composition of Vesta. Heat conducts upward through the lid to a cold surface, cooling the magma ocean beneath. This calculation gives the heat flux coming out of the magma ocean into the crust. As Fig. 4A in the main text indicates, heat flux through the conductive lid is sufficient to drive superadiabatic heat loss from the core in every case considered, and for a significant amount of time.

As heat conducts through the lid, the underlying magma ocean is cooled. As the body cools, the magma ocean temperature drops and eventually will reach a temperature at which the ratio of solid to liquid is sufficiently high to further inhibit convection. We estimate this temperature to be ~850°C: as solidification proceeds, the solidus temperature of residual liquids drops, so although the bulk body's silicate composition would be solid at 850°C, evolved liquids will not be. We find this will occur after ~3 m.y., ~5-20 m.y., and ≥~30 m.y., respectively, for 70 km, 200 km, and 500 km radius bodies. These times should be viewed as lower limits because the heat flux would drop drastically as crystal fraction rises, and this effect is not included in our calculations. This effect would also mean that the core heat fluxes shown in Fig. 4A are overestimates when the temperature approaches 850°C.

6.2. Conditions for dynamo action. Superadiabatic heat flux out of the core is likely a necessary but not sufficient condition for dynamo action. To further test the hypothesis that early planetesimals could generate angrite-like dynamos, we estimated the magnetic Reynolds numbers (Re_m, ratio of field generation to field diffusion) and expected surface fields on bodies with a wide range of properties like that represented by asteroids today (Table S5).

To generate a self-sustaining dynamo, Re_m must exceed some critical bound that is at least unity. A theoretical argument gives the bound $Re_m > \pi$ where Re_m is based on the maximum fluid velocity (*S99*). This bound would suggest that Re_m >1 is a

reasonable estimate for critical dynamo action if Re_m is calculated from the characteristic rather than maximum fluid velocity.

We estimated $Re_m \sim ur_c/\eta$, where u is the characteristic fluid velocity, r_c is the core radius, and η is the magnetic diffusivity. Because all the bodies considered here (Table S5) are rapid rotators, we assume their dynamos are in magnetostrophic balance (*S94*) to estimate u:

$$u = \left(\frac{\alpha_T g F_{conv}}{C_p \rho_c \Omega} \right)^{0.5}$$

where $F_{conv} = F_{tot} - F_{cond}$ is the core convective heat flux for a total core heat flux F_{tot}, ρ_c is the core density (see Table S5), and Ω is the angular rotational velocity of the planet (specified by the rotation period in Table S5). Other scaling relations between convective heat flux and fluid velocity generally give larger values, so the velocity estimates we use here are conservative. We estimate the core field strength for unity Elsasser and magnetic Reynolds numbers as:

$$B_0 = \sqrt{2\Omega\rho_c/\sigma}$$

for electrical conductivity $\sigma \sim 5\times10^4$ S m^{-1} at the pressures expected in our planetesimal cores (*S100*) (this number is not well constrained). If we further assume that the dipole field is $B_{dip} = 0.1B_0$ at the core-mantle boundary (similar to the Earth's value), then using the fact that the dipole will decay as $(r_c/r)^3$ we can estimate the surface fields for r = planetary radius. As shown in Fig. 4B there are many combinations of parameters that can produce an APB dynamo and angrite-like surface fields for bodies with radii > 80 km.

7.0. Implications for the Mercury hypothesis

Irving and Kuehner (*S101*) and Kuehner et al. (*S102*) have postulated that the angrites are samples of the planet Mercury. Our mean paleointensity values are ~50 times higher than Mercury's surface field today (*S103*). However, this does not rule out Mercury as the angrite parent body because the angrites record fields from long ago. Mercury's present weak surface field has been attributed to the possibility that its dynamo operates in a thin shell regime due to a high mass ratio of the solid core to the liquid core (*S104*). We might expect early Mercury to have had a core that contained relatively more liquid than that today. Our dynamo calculations suggest that a thick shell ancient Mercury dynamo could generate angrite-like paleointensities. Therefore, our angrite paleointensities may in fact be consistent with an origin on ancient Mercury.

Table S1. Summary of Hysteresis Data for Angrites

Meteorite	Sample	Mass (mg)	X_p ($\times 10^{-5}$ Am^2T^{-1})	M_{rs} ($\times 10^{-8}$ Am^2)	M_s ($\times 10^{-7}$ Am^2)	H_c (mT)	M_{rs}/M_s	H_{cr}/H_c
D'Orbigny	11	51	1.8	58.0	20.9	17.5	0.27	1.55
	12	24	0.69	26.1	10.0	18.0	0.26†	1.51
A-881371	,63	66	1.9	34.1	16.2	16.3	0.21	1.72
Angra dos Reis	M2	90*	0.19	7.58	8.29	13.5	0.09†	2.65
	3S1	20	0.26	2.28	3.01	15.0	0.08	6.42

Note: Shown is a summary of room-temperature hysteresis data measured with a DMS vibrating sample magnetometer at room temperature. The first column gives the meteorite name, the second column gives the subsample name, the third column gives the sample mass, the fourth column gives the paramagnetic susceptibility as estimated from the high-field slope, the fifth column gives the saturation remanent moment, the sixth column gives the saturation moment, the seventh column gives the coercivity, the eighth column gives the computed squareness (ratio of saturation remanent magnetization to saturation magnetization) and the ninth column gives the ratio of coercivity of remanence (see Table S2) to coercivity.

*****Mass of this subsample is approximate (within a factor of 2 of actual mass) because it was weighed following thermomagnetic analyses.

†Subsamples taken from these samples were later subjected to thermomagnetic analyses (Fig. S9A,B). Hysteresis measurements taken before and after the thermomagnetic analyses (Fig. S9C,D) measured M_{rs}/M_s of 0.27 (before) and 0.23 (after) for the subsample taken from D'Orbigny 12 and 0.13 (before) and 0.30 (after) for the subsample taken from Angra dos Reis M2.

Table S2. Summary of Rock Magnetic Remanence Data for Angrites

Meteorite	Sample	S ratio	*R*	MDF ARM (mT)	MDF IRM (mT)	L-F Test	H_{cr} (mT)
D'Orbigny	11	0.95	0.33	15.3	18.2	H	27.2
	12	0.96	0.32	15.9	18.1	L/H	27.2
	F1	0.96	0.32	16.2	19.1	H	29.3
	F2	0.95	0.27	18.0	18.3	L/H	35.9
	F6	0.97	0.30	15.4	16.4	H	27.3
	FB8	0.95	0.31	16.1	18.0	L/H	27.8
	FB10AA	0.96	0.32	13.6	15.8	H	24.7
	FB10AB	0.95	0.31	17.3	18.2	L/H	28.9
	FB10B	0.96	0.32	15.3	18.0	H	28.0
	FB14	0.96	0.31	15.0	15.9	H	25.7
A-881371	,63	0.97	0.30	15.1	17.1	H	27.9
Angra dos Reis	M3	0.38	0.40	17.6	40.6	L	73.4
	M4	0.40	0.42	16.4	29.6	L	52.5
	M6	0.47	0.39	18.9	30.0	L	58.6
	M7	0.33	0.40	18.4	51.7	L/H	94.0
	3S1	0.34	0.39	15.2	52.6	L/H	96.3
	AMC3	0.78	0.31	18.6	20.4	L	31.9
	AMC16	0.82	0.32	18.0	19.2	L	27.8

Note: Shown is a summary of room temperature rock magnetic remanence data measured with the 2G Superconducting Rock Magnetometer. The first column gives the meteorite name, the second column gives the subsample name, the third column gives the S ratio = - ($IRM_{-300\ mT}/IRM_{900\ mT}$) following (*S19, 20*), the fourth column gives the Cisowski *R* value (*S16*), the fifth column gives the mean destructive field for an ARM acquired in 200 mT peak AF field with 2 mT DC bias field, the sixth column gives the mean destructive field for an IRM_{200mT}, the seventh column gives the outcome of the Lowrie-Fuller test (*S18*) (L = low field remanence/ARM more stable, H = high field remanence/IRM more stable, L/H = ARM equally stable to IRM), and the eighth column gives the coercivity of remanence. Masses for all samples here except for D'Orbigny FB10AB (which has a mass of 2.1 mg) are listed in Table S3.

Table S3. Summary of Paleointensity Estimates for High Coercivity (HC) Components in Angrites

Meteorite	Sample	Source	Mass (mg)	ARM Paleointensity (μT)			IRM Paleointensity (μT)
				50 μT bias	200 μT bias	600 μT bias	
D'Orbigny	F1	PS	75	12±3	15±3	13±3	9.6±2
	F2	PS	10	10±5	18±4	17±4	15±3
	F6	MT	75	9.2±4	11±3	10±2	7.7±2
	11	MT	51	14±10	20±7	12±4	17±5
	12	MT	24	17±15*	17±21*	26±23*	21±18
	FB8	MT	22	26±12	24±5	25±5	21±5
	FB10AA	MT	28	7.2±18	18±15	20±17	16±14
	FB10B	MT	21	29±18	26±17	22±16	20±14
	FB14	MT	163	8.8±3	13±4	14±4	12±4
A-881371	,63	NIPR	66	2.5±1† 8.1	2.5±0.9† 6.9	2.7±1† 7.1	2.1±0.8† 2.2
Angra dos Reis	M3	MNB	20	7.2±6	6.9±5	7.1±5	7.8±5
	M4	MNB	7	16±9	13±6	13±6	22±8
	M6	MNB	40	6.2±7† 12	7.3±8† 11	7.3±8† 11	11±11† 5.1
	M7	MNB	70	36±5	28±2	28±2	35±3
	3S1	MNB	20	2.8±9*	41±23*	31±23*	16±14
	AMC3	AMNH	58	20±0.9	17±0.7	15±0.5	21±1.2
	AMC16	AMNH	76	17±0.9	16±0.4	15±0.3	22±0.5

Note: Shown are paleointensity estimates for HC components measured during this study. The first column gives the meteorite name, the second column gives the subsample name, the third column gives the source of the sample (PS = private source, MT = La Memoire de la Terre, NIPR = National Institute of Polar Research, Japan, MNB = Museu Nacional, Brasil, AMNH = American Museum of National History), the fourth column gives the sample mass, the fifth column gives the paleointensity estimate using the ARM method (assuming paleointensity in microteslas = (NRM/ARM)/2 × (bias field in microteslas) as typical for pseudo single domain grains) (*S78, 88*), and the final column gives the paleointensity estimate using the IRM method (assuming paleointensity in microteslas = NRM/IRM x 3000) (*S1, 76*). The given uncertainties are formal 95% confidence intervals associated with least squares fitting to the paleointensity plots. The actual uncertainty for each value is estimated to be a factor of ~3 primarily due to the poorly known ratio of IRM and ARM to thermoremanence.

*ARM paleointensities for these two samples were measured after saturation IRM experiments and therefore have high uncertainty.

†These samples exhibited high-AF noise which obscures decay of the magnitude of the NRM vector at high AF values. Therefore, two paleointensity estimates are reported for these samples. The first row gives the estimate derived from the least squares slope observed in the NRM-ARM and NRM-IRM demagnetization plots (the same technique used to calculate other values in this table). The second row gives the values calculated by taking the ratio of the NRM remaining after removal of the

LC component to the ARM and IRM after removal of the LC component. The latter should be less affected by ARM-related noise but lacks confidence intervals because it is not a least squares fit.

Table S4. Parameters Used to Calculate Core Heat Fluxes for Model Planetesimals

Parameter	Values
Planetesimal radius	70, 200, and 500 km
Core radius for 70, 200 and 500 km bodies	10, 63, and 350 km
Thickness of conductive lid for 70 km body	30, 20, and 10 km
Thickness of conductive lid for 200 km body	50, 40, 30, 20, and 10 km
Thickness of conductive lid for 500 km body	100, 80, 60, 40, and 20 km
Initial temperature at base of crust	1100°C
Temperature at surface	-23°C
Density of the magma ocean	3000 kg m^{-3}
Density of the mafic crust	3200 kg m^{-3}
Thermal diffusivity	1×10^{-6} m^2 s^{-1}
Heat capacity of silicates	1260 J kg^{-1} K^{-1}

Table S5. Range of Parameters Used to Calculate Re_m and Surface Fields for Model Planetesimals

Parameter	Values
Planetesimal radius	10, 20, 40, 60, 80, 100, 120, 140, 160,180 and 200 km
Core mass fraction	0.08, 0.2, 0.3, 0.4, 0.5 and 0.6
Rotation period	6, 12, 24, 48, 72 h
Average core density	5000, 600, 7000, 8000 kg m^{-3}
Average mantle density	1000, 2000, and 3000 kg m^{-3}
Total heat flux	0.01, 0.03, 0.05, 0.1, 0.2, 0.3, 0.4 W m^{-2}

References

S1. J. Gattacceca, P. Rochette, *Earth Planet. Sci. Lett.* **227**, 377 (2004).
S2. D. W. Collinson, *Meteorit. Planet. Sci.* **32**, 803 (1997).
S3. P. Wasilewski, T. Dickinson, *Meteorit. Planet. Sci.* **35**, 537 (2000).
S4. J. L. Kirschvink, R. E. Kopp, T. D. Raub, *Geochem. Geophys. Geosyst.* **9**, Q05Y01 (2008).
S5. D. Potter, K., A. Stephenson, *J. Geophys. Res.* **95**, 15573 (1990).
S6. D. Potter, K., A. Stephenson, *Geophys. Res. Lett.* **17**, 2437 (1990).
S7. G. J. Borradaile, F. Lagroix, D. Trimble, *Geophys. J. Int.* **147**, 176 (2001).
S8. P. H. M. Dankers, J. D. A. Zijderveld, *Earth Planet. Sci. Lett.* **53**, 89 (1981).
S9. A. Stephenson, *J. Geophys. Res.* **98**, 373 (1993).
S10. C. Snape, *Geophys. J. R. Astr. Soc.* **23**, 361 (1971).
S11. E. A. Hailwood, L. Molyneux, *Geophys. J. R. Astr. Soc.* **39**, 421 (1974).
S12. D. W. Collinson, *Methods in Rock Magnetism and Paleomagnetism*. (Chapman and Hall, New York, N.Y., 1983), pp. 503.
S13. S. J. Morden, *Phys. Earth. Planet. Inter.* **71**, 189 (1992).
S14. G. Acton *et al.*, *J. Geophys. Res.* **112**, doi:10.1029/2006JB004655 (2007).
S15. D. J. Dunlop, *J. Geophys. Res.* **107**, doi:10.1029/2001JB000486 (2002).
S16. S. Cisowski, *Phys. Earth Planet. Inter.* **26**, 56 (1981).
S17. W. Lowrie, M. Fuller, *J. Geophys. Res.* **76**, 6339 (1971).
S18. S. Xu, D. J. Dunlop, *J. Geophys. Res.* **100**, 22533 (1995).
S19. P. P. Kruiver, H. F. Passier, *Geochem. Geophys. Geosyst.* **2**, 2001GC000181 (2001).
S20. R. Thomson, F. Oldfield, *Environmental Magnetism*. (Allen and Unwin, Concord, 1986), pp. 227.
S21. R. J. Harrison, A. Putnis, *Am. Mineral.* **81**, 375 (1996).
S22. U. Golla-Schindler, H. S. C. O'Neill, A. Putnis, *Am. Mineral.* **90**, 1278 (2005).
S23. M. Robbins, G. K. Wertheim, R. C. Sherwood, D. N. E. Buchanan, *J. Phys. Chem. Sol.* **32**, 717 (1971).
S24. T. Nagata, *Rock Magnetism*. (Maruzen Company, Tokyo, 1961), pp. 350.
S25. S. Klemme, H. S. C. O'Neill, W. Schnelle, E. Gmelin, *Am. Mineral.* **85**, 1686 (2000).
S26. G. Kurat *et al.*, *Geochim. Cosmochim. Acta* **68**, 1901 (2004).
S27. T. Nagata, *Proc Lunar Planet. Sci. Conf. 13*, A779 (1983).
S28. P. Wasilewski, *Phys. Earth Planet. Inter.* **52**, 150 (1988).
S29. R. S. Clarke, E. R. D. Scott, *Am. Mineral.* **65**, 624 (1980).
S30. D. E. Watson, E. E. Larson, J. M. Herndon, M. W. Rowe, *Earth Planet. Sci. Lett.* **27**, 101 (1975).
S31. J. M. Herndon, M. W. Rowe, E. E. Larson, D. E. Watson, *Earth Planet. Sci. Lett.* **29**, 283 (1976).
S32. P. J. Wasilewski, C. Saralker, *Proc. Lunar Planet. Sci. Conf. 12*, 1217 (1981).
S33. M. Prinz *et al.*, *Earth Planet. Sci. Lett.* **35**, 317 (1977).
S34. D. J. Dunlop, O. Ozdemir, *Rock Magnetism: Fundamentals and Frontiers*. Cambridge Studies in Magnetism (Cambridge University Press, New York, 1997), pp. 573.

S35. D. W. Mittlefehldt, in *Treatise on Geochemistry,* H. D. Holland, K. K. Turekian, Eds. (Elsevier, 2007), vol. 1, pp. 1-40.
S36. M. E. Varela *et al.*, *Geochim. Cosmochim. Acta* **67**, 5027 (2003).
S37. T. Mikouchi, M. Miyamoto, G. McKay, *Proc. NIPR Symp. Antarc. Meteorites* **9**, 174 (1996).
S38. G. McKay, *Lunar Planet. Sci. 20*, 677 (1989).
S39. G. McKay, D. Lindstrom, S.-R. Yang, J. Wagstaff, *Lunar Planet. Sci. 19*, 762 (1988).
S40. A. Jambon *et al.*, *Meteorit. Planet. Sci.* **40**, 361 (2005).
S41. P. Rochette *et al.*, *Meteorit. Planet. Sci.*, submitted (2008).
S42. B. P. Weiss, L. E. Fong, H. Vali, E. A. Lima, F. Baudenbacher, *Geophys. Res. Lett.*, submitted (2008).
S43. B. P. Weiss *et al.*, *Proc. Natl. Acad. Sci. USA* **101**, 8281 (2004).
S44. P. Rochette *et al.*, *Meteorit. Planet. Sci.* **40**, 529 (2005).
S45. T. Mikouchi, M. Miyamoto, G. McKay, L. Le, *Met. Soc. 64*, abstract #5344 (2001).
S46. C. E. G. Bennett, J. Graham, *Am. Mineral.* **66**, 1254 (1980).
S47. P. H. Warren, A. M. Davis, *Antarct. Meteorites XX*, 257 (1995).
S48. M. E. Varela *et al.*, *Meteorit. Planet. Sci.* **40**, 409 (2005).
S49. C. Floss, G. Crozaz, G. McKay, T. Mikouchi, M. Killgore, *Geochim. Cosmochim. Acta* **67**, 4775 (2003).
S50. D. W. Mittlefehldt, M. Killgore, M. T. Lee, *Meteorit. Planet. Sci.* **37**, 345 (2002).
S51. G. Pullaiah, G. Irving, K. L. Buchan, D. J. Dunlop, *Earth Planet. Sci. Lett.* **28**, 133 (1975).
S52. D. J. Dunlop, O. Ozdemir, D. A. Clark, P. W. Schmidt, *Earth Planet. Sci. Lett.* **176**, 107 (2000).
S53. B. P. Weiss *et al.*, *Science* **290**, 791 (2000).
S54. I. Garrick-Bethell, B. P. Weiss, *Lunar Planet. Sci. 37*, abstract #2413 (2006).
S55. O. A. Derby, *Revista do Observatorio* **3**, 33 (1888).
S56. A. Weigel, O. Eugster, C. Koeberl, U. Krahenbuhl, *Geochim. Cosmochim. Acta* **61**, 239 (1997).
S57. K. L. Louzada *et al.*, *Earth Planet. Sci. Lett.*, in press (2008).
S58. M. Prevot, *Geophys. J. R. Astr. Soc.* **66**, 169 (1981).
S59. D. J. Dunlop, *Geophys. J. R. Astr. Soc.* **69**, 763 (1982).
S60. W. Lowrie, *Nature* **243**, 27 (1973).
S61. D. J. Dunlop, *Rev. Geophys. Space Phys.* **11**, 855 (1973).
S62. B. M. Moskowitz, *Geophys. J. R. Astr. Soc.* **82**, 143 (1985).
S63. D. J. Dunlop, *Geophys. J. R. Astr. Soc.* **74**, 667 (1983).
S64. J. M. Hall, C. C. Walls, S. L. Hall, *Phys. Earth Planet. Inter.* **88**, 101 (1995).
S65. J. A. Bowles, H. P. Johnson, *Geophys. Res. Lett.* **26**, 2279 (1999).
S66. Y. Yu, L. Tauxe, *Phys. Earth Planet. Inter.* **159**, 32 (2006).
S67. T. Kohout, G. Kletetschka, F. Donadini, M. Fuller, E. Herrero-Bervera, *Stud. Geophys. Geod.* **52**, 225 (2008).
S68. G. Kletetschka, M. H. Acuna, T. Kohout, P. J. Wasilewski, J. E. P. Connerney, *Earth Planet. Sci. Lett.* **226**, 521 (Oct 15, 2004).

S69. G. Kletetschka, T. Kohout, P. J. Wasilewski, *Meteorit. Planet. Sci.* **38**, 399 (Mar, 2003).
S70. M. Fuller *et al.*, *Geophys. Res. Lett.* **15**, 518 (1988).
S71. M. Fuller, S. M. Cisowski, in *Geomagnetism,* J. A. Jacobs, Ed. (Academic Press, Orlando, 1987), vol. 2, pp. 307-455.
S72. M. Fuller, T. Kidane, J. Ali, *Phys. Chem. Earth* **27**, 1169 (2002).
S73. G. Kletetschka *et al.*, *Phys. Earth. Planet. Inter.* **154**, 290 (2006).
S74. V. Verrier, P. Rochette, *Geophys. Res. Lett.* **29**, art. no. (Sep 15, 2002).
S75. Y. Yu, L. Tauxe, J. S. Gee, *Earth Planet. Sci. Lett.* **162**, 244 (2007).
S76. Y. J. Yu, *Earth Planet. Sci. Lett.* **250**, 27 (2006).
S77. K. Lawrence, C. Johnson, L. Tauxe, J. Gee, *Phys. Earth Planet. Inter.*, doi:10.1016/j.pepi.2008.05.007 (2008).
S78. A. Stephenson, D. W. Collinson, S. K. Runcorn, *Proc. Tenth Lunar Planet. Sci. Conf.*, 2859 (1974).
S79. A. Stephenson, S. K. Runcorn, D. W. Collinson, *Proc Lunar Planet Sci. Conf. 8*, 679 (1977).
S80. K. A. Hoffmann, J. R. Baker, S. K. Banerjee, *Phys. Earth Planet. Inter.* **20**, 317 (1979).
S81. C. M. Carmichael, *Phys. Earth Planet. Inter.* **13**, 332 (1977).
S82. N. Sugiura, D. W. Strangway, *Proc. Lunar Planet. Sci. Conf. 11th*, 1801 (1980).
S83. S. J. Morden, *Meteoritics* **27**, 560 (1992).
S84. M. E. Bailey, D. J. Dunlop, *Phys. Earth. Planet Inter.* **13**, 360 (1977).
S85. M. Kono, *Geophys. J. R. Astr. Soc.* **54**, 241 (1978).
S86. D. J. Dunlop, M. E. Bailey, M. F. Westcott-Lewis, *Proc. Lunar Sci. Conf. 6*, 3063 (1975).
S87. S. Levi, M. T. Merrill, *Earth Planet. Sci. Lett.* **32**, 171 (1976).
S88. D. J. Dunlop, K. S. Argyle, *J. Geophys. Res.* **102**, 20199 (1997).
S89. R. L. Hartstra, *Geophys. J. R. Astr. Soc.* **73**, 719 (1983).
S90. S. W. Weisberg, *Applied Linear Regression*. (John Wiley & Sons, New York, 1985), pp. 324.
S91. P. A. Selkin, J. S. Gee, L. Tauxe, W. P. Meurer, A. J. Newell, *Earth Planet. Sci. Lett.* **183**, 403 (2000).
S92. P. J. Hevey, I. S. Sanders, *Icarus* **41**, 95 (2006).
S93. T. McCoy, D. W. Mittlefehldt, L. Wilson, in *Meteorites and the Early Solar System II,* D. Lauretta, H. Y. McSween, Eds. (Univ. of Arizona Press, Tucson, 2003), pp. 733-745.
S94. D. J. Stevenson, *Earth Planet. Sci. Lett.* **208**, 1 (2003).
S95. F. D. Stacey, O. L. Anderson, *Phys. Earth. Planet. Inter.* **124**, 153 (2001).
S96. D. R. Stegman, A. M. Jellinek, S. A. Zatman, J. R. Baumgardner, M. A. Richards, *Nature* **421**, 143 (Jan 9, 2003).
S97. K. S. Bartels, T. L. Grove, *Proc. Lunar Planet Sci. Conf. 21*, 351 (1991).
S98. N. Sugiura, A. Miyazaki, Q. Z. Yin, *Earth Planets Space* **58**, 1079 (2006).
S99. P. H. Roberts, D. Gubbins, in *Geomagnetism,* J. A. Jacobs, Ed. (Academic Press, London, 1987), vol. 2, pp. 185-249.
S100. R. A. Secco, H. H. Schloessin, *J. Geophys. Res.* **94**, 5887 (1989).

S101. A. J. Irving, S. M. Kuehner, *Workshop on Chronology of Meteorites and the Early Solar System*, abstract #4050 (2007).
S102. S. M. Kuehner *et al.*, *Lunar Planet. Sci. 37*, abstract #1344 (2006).
S103. N. F. Ness, *Annu. Rev. Earth Planet. Sci* **7**, 249 (1979).
S104. S. Stanley, J. Bloxham, W. E. Hutchison, M. T. Zuber, *Earth Planet. Sci. Lett.* **234**, 27 (2005).

Figure Captions

Figure S1. Magnetization directions of mutually oriented subsamples of angrites. Shown for each angrite are least squares fits to each subsample and associated uncertainty ellipse. The diameter of each uncertainty ellipse has been set to either the mean angular deviation (MAD) of the associated least squares fit or else the ~10° orientation uncertainty (whichever is greater). Fisher mean direction (red star) and associated 95% uncertainty confidence estimate (α_{95}) are shown for interior subsamples. (A) Angra dos Reis parent sample from the Museu Nacional, Brasil. Mean direction for interior samples M3, M4, M6, M7 and M9 has α_{95} = 28.1° and estimated precision parameter k = 6.7. (B) D'Orbigny parent sample FB. Mean direction for interior samples FB8, FB10AA, FB10AB, FB10B, and FB14 has α_{95} = 24.9° and estimated precision parameter k = 8.3.

Figure S2. Paleointensity experiments on D'Orbigny sample F1 and Angra dos Reis sample AMC16 (see Fig. 1C). (A) Anhysteretic remanent magnetization (ARM) method for D'Orbigny sample F1, in which cumulative ARM acquired in laboratory DC bias fields of 0.05 mT (squares), 0.2 mT (circles), and 0.6 mT (diamonds) superimposed on stepwise increasing alternating field (AF) is plotted as a function of the peak AF. Data points from LC and HC components are colored blue and red, respectively. The HC component is estimated to have been acquired in a field of 12 ± 3 μT (0.05 mT bias field), 15 ± 3 μT (0.2 mT bias field) and 13 ± 3 μT (0.6 mT bias field) (uncertainties are formal 95% confidence interval derived from linear regression). (B) Isothermal remanent magnetization (IRM) method on D'Orbigny sample F6, in which cumulative AF demagnetization of a saturating IRM is plotted as a function of peak AF. Data points from LC and HC components are colored blue and red, respectively. The HC component is estimated to have been acquired in a field of 10 ± 2 μT. (C) ARM paleointensity for Angra dos Reis sample AMC16 for laboratory DC bias fields of 0.05 mT (squares), 0.2 mT (circles), and 0.6 mT (diamonds). The HC component is estimated to have been acquired in a field of 17 ± 0.9 μT (0.05 mT bias field), 16 ± 0.4 μT (0.2 mT bias field) and 15 ± 0.3 μT (0.6 mT bias field). (D) IRM paleointensity on Angra dos Reis sample AMC16, in which cumulative AF demagnetization of a saturating IRM is plotted as a function of peak AF. The HC component is estimated to have been acquired in a field of 22 ± 0.5 μT.

Figure S3. Alternating field (AF) demagnetization and paleointensity data for A-881371 sample ,63 (A) Equal area plot showing direction of magnetization vector. Black dots are single measurements (shown for all steps between NRM and AF 11.0 mT). Red dots are mean directions for multiple steps calculated for six AF bins: AF 9.0 to 11.2 mT (11 steps), AF 11.4 to 18.4 mT (30 steps), AF 18.8 to 25.7 (20 steps), AF 26.4 to 37.4 (20 steps), AF 38.4 to 52.8 (19 steps), and AF 55.0-155.0 mT (21 steps). Between NRM and AF 8.7 mT, a relatively strong low coercivity overprint is removed, reflected by motion of the remanence vector (arrow). Above, AF 8.7 mT, the mean direction is approximately stationary around the 8.7 mT direction but with a wide dispersion due to spurious ARM from our AF system. (B) AF demagnetization from 7.2-200 mT of a laboratory ARM (200 mT peak AC field with 7 μT DC bias field in direction given by

star) intended as a model thermoremanence acquired in a field of 3.5 μT. Sample directions are averaged as in (A). Observed scatter is similar to that observed during AF of NRM, with laboratory ARM essentially lost in the noise by AF 150 mT. (C) ARM paleointensity experiment with 0.2 mT bias field. ARM paleointensity experiments were also conducted in 0.05 and 6 mT bias fields (data not shown for clarity). Inferred paleointensity was 2.5 ± 0.9 μT (95% confidence interval from regression). (D) IRM paleointensity experiment. Inferred paleointensity was 2.1 ± 0.8 μT.

Figure S4. Room temperature hysteresis loops for selected samples. Shown is the sample moment as a function of applied field. (A) D'Orbigny sample 11. (B) A-881371 sample ,63. (C) Angra dos Reis sample 3S-1. The contribution from paramagnetic susceptibility as estimated from the high-field slope (Table S1) has been subtracted from these data.

Figure S5. Anhysteretic remanent magnetization (ARM) acquisition experiments on selected characteristic samples. Shown is the ARM acquired in a 200 mT AC field as a function of DC bias field. Lower dotted curve is that of highly interacting chiton tooth magnetite and upper dotted curve is noninteracting magnetite in magnetotactic bacteria. (A) D'Orbigny sample F6. (B) A-881371 sample ,63. (C) Angra dos Reis sample M6.

Figure S6. Lowrie-Fuller tests for selected samples. Shown is alternating field demagnetization of an anhysteretic remanent magnetization (ARM) acquired in a 200 mT peak AC field with 0.2 mT DC bias field (light blue symbols) and of an isothermal remanent magnetization (IRM) acquired in a 200 mT field. Both curves are normalized to the starting value just prior to AF demagnetization. (A) D'Orbigny sample F6. (B) A-881371 sample ,63. (C) Angra dos Reis sample M6.

Figure S7. Isothermal remanent magnetization (IRM) acquisition and demagnetization experiments on selected samples. (A) IRM acquisition and alternating field (AF) demagnetization of IRM by D'Orbigny sample F6. Both curves are normalized to the highest-field IRM value. (B) Derivative of IRM acquisition (purple crosses) and AF demagnetization of IRM (light blue crosses) for D'Orbigny sample F6, with running average given by solid lines. (C) IRM acquisition and AF of IRM for A-881371 sample ,63. (D) Derivatives of IRM acquisition and AF of IRM for A-881371 sample ,63. (E) IRM acquisition and AF of IRM for Angra dos Reis sample M4. (F) Derivatives of IRM acquisition and AF of IRM for Angra dos Reis sample M4.

Figure S8. Low temperature cycling of selected samples. Each sample was briefly exposed to a saturating field (4 T) at room temperature. The sample moment was then progressively measured during cycling down to 10 K and back up to room temperature. in a near-zero (<0.2 mT) field. (A) D'Orbigny sample 11. (B) A-8813171 sample ,63. (C) Angra dos Reis sample M2.

Figure S9. Thermomagnetic data for selected samples. Shown is the sample moment during heating and cooling from room temperature to 702°C. Samples were exposed to a 1 T field at room temperature prior to starting the measurements. (A) Subsample taken

from D'Orbigny sample 12. (B) Subsample taken from Angra dos Reis sample M2. (C) Room temperature hysteresis loops taken for subsample in (A) before (blue points) and after (black points) thermomagnetic treatment. (D) Room temperature hysteresis loops taken for subsample in (B) before (blue points) and after (black points) thermomagnetic treatment.

Figure S10. Backscatter electron microscopy imaging of D'Orbigny sample FB14. (A) Intergrowth of troilite (tr) (FeS) with near-end member magnetite (mt) ($Fe_{2.9}Z_{0.1}O_4$ where Z = various impurities), and Al-Ti magnetite (Ti-mt) ($Fe_{2.0}Al_{0.7}Ti_{0.3}O_4$). Surrounding phases are anorthite (an), Ca-rich olivine (ol), and Al-Ti-diopside-hedenbergite (cpx). Scale bar is 30 μm. (B) Intergrowth of troilite with near-end member magnetite surrounded by olivine. Scale bar is 10 μm.

Figure S11. Viscous remanent magnetization (VRM) experiments on angrites. Samples were exposed to Earth's field for time given by star and then returned to our shielded room (<150 nT) where their moments were semi-continuously measured as they viscously decayed. (A) Intensity of Angra dos Reis interior sample M7. After 15 d, the sample decayed to the pre-VRM moment intensity (noted by asterisk). A least squares regression to data for $t \geq 154$ s gave a magnetic viscosity decay coefficient $S_d = dM/d(\log t) = 8.2\times10^{-12}$ Am^2 (log s)$^{-1}$. (B) Direction of Angra dos Reis interior sample M7. Sample had acquired a component in the direction of the Earth's field and decayed to the original pre-VRM direction after 15 d. (C) A-881371 sample ,63. (D) D'Orbigny sample 11.

Figure S12. Magnet contamination test for Angra dos Reis sample M7. Following analysis and demagnetization of the NRM, the sample was given an artificial remanence consisting of an anhysteretic remanent magnetization (ARM) in a peak AC field of 200 mT and a DC bias field of 50 μT (equivalent to a thermoremanence acquired in 36 μT field assuming the ratio of thermoremanence to ARM = 2) overprinted by an isothermal remanent magnetization (IRM) acquired in a 21.6 mT DC field (equal to the inferred IRM magnet overprint on this sample). (A) AF demagnetization of artificial remanence up to 83.6 mT. Shown is a two dimensional projection of the endpoint of the magnetization vector. Closed (open) symbols represent end points of magnetization projected onto horizontal (vertical) planes. (B) Close-up of AF demagnetization shown in (A) for fields above 16.8 mT. (C) ARM paleointensity experiment for artificial remanence shown in (A) and (B). (D) IRM paleointensity experiment for artificial remanence shown in (A) and (B). Peak fields for selected AF demagnetization steps are labeled in each plot.

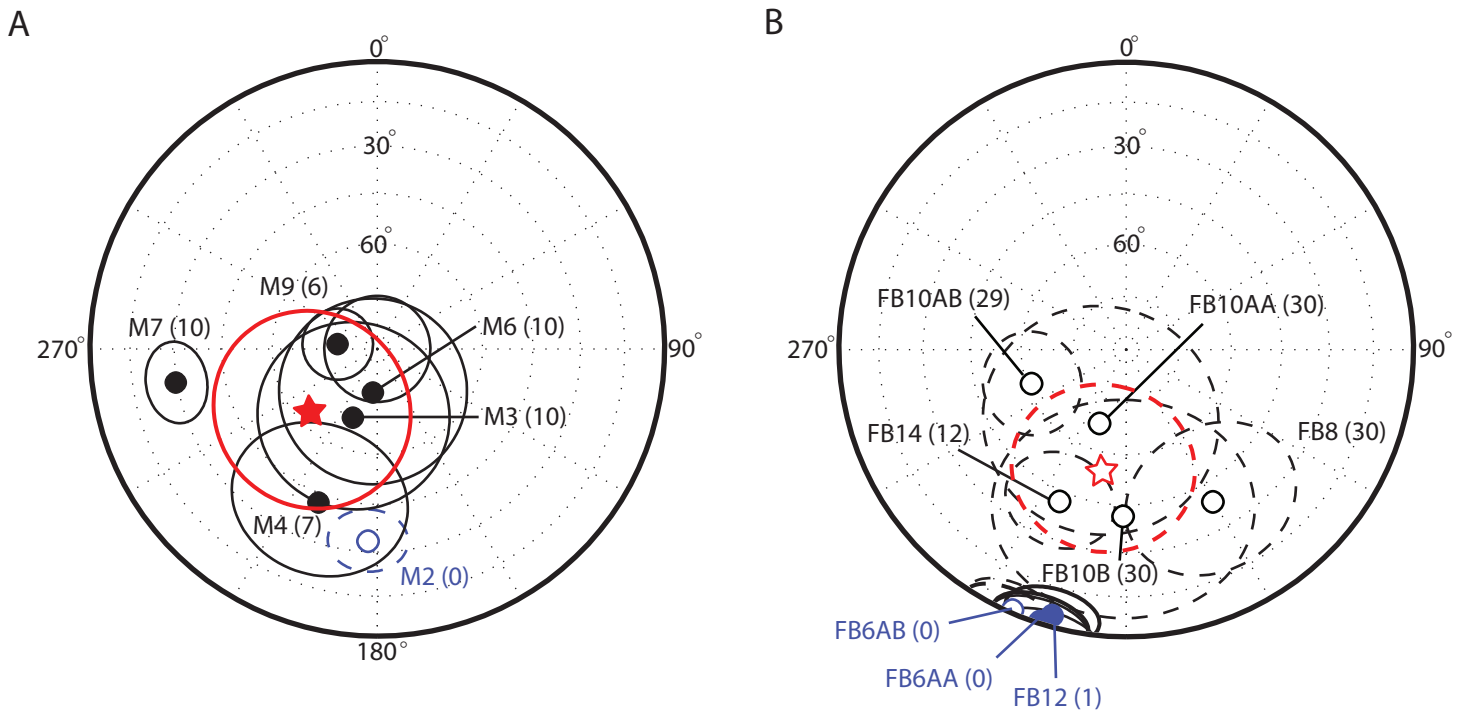

Weiss et al. 2008 Figure S1

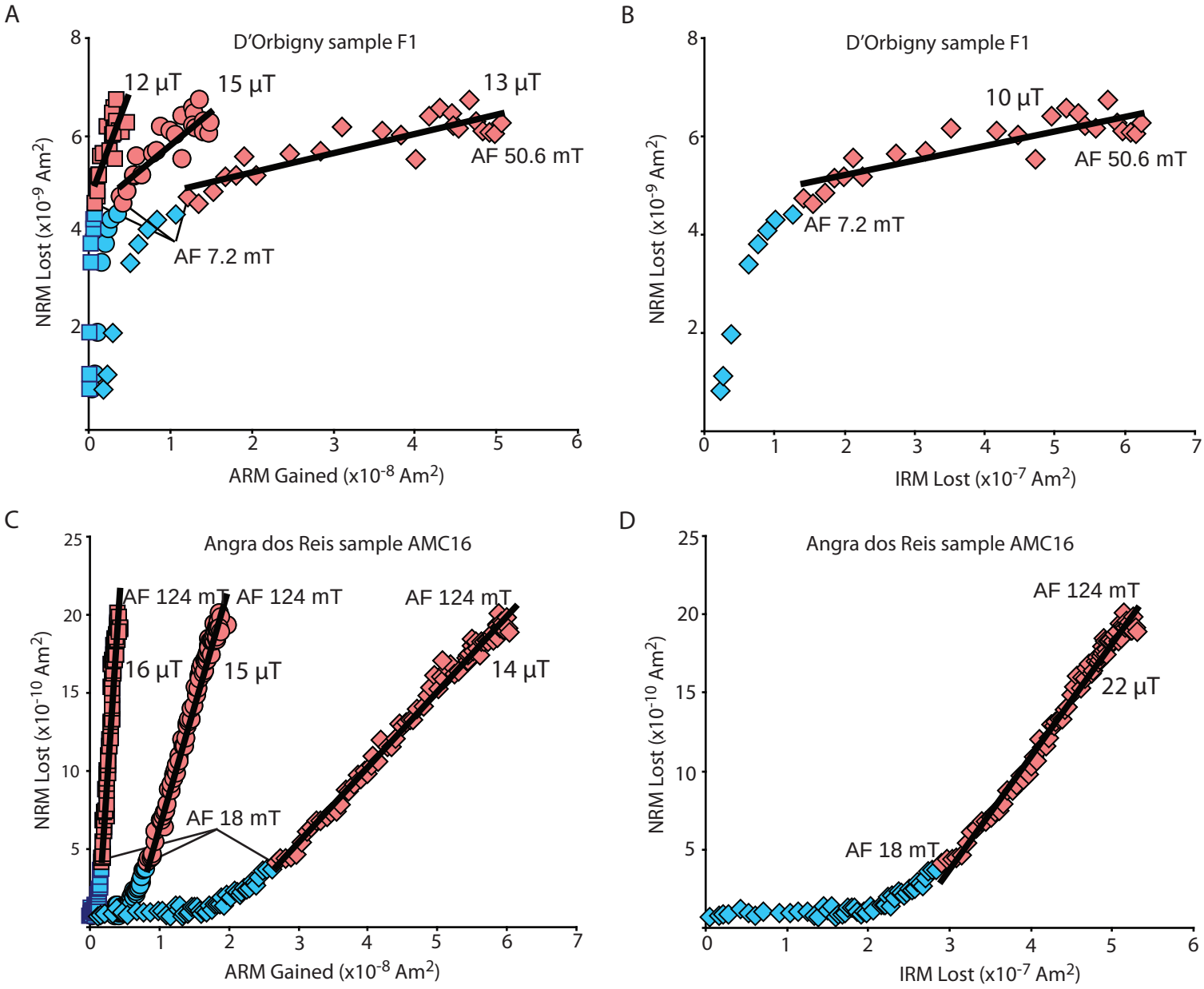

Weiss et al. 2008 Figure S2

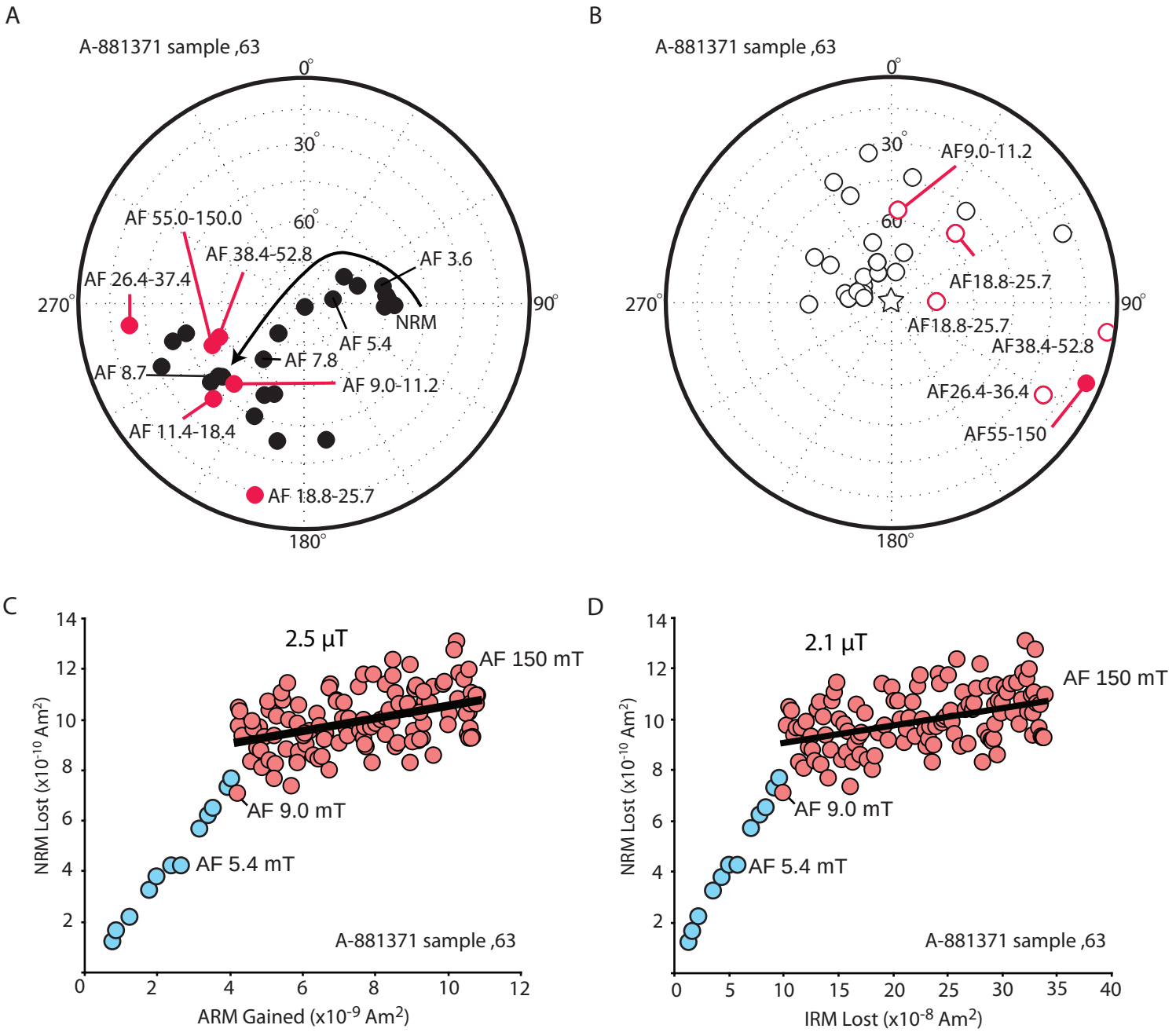

Weiss et al. 2008 Figure S3

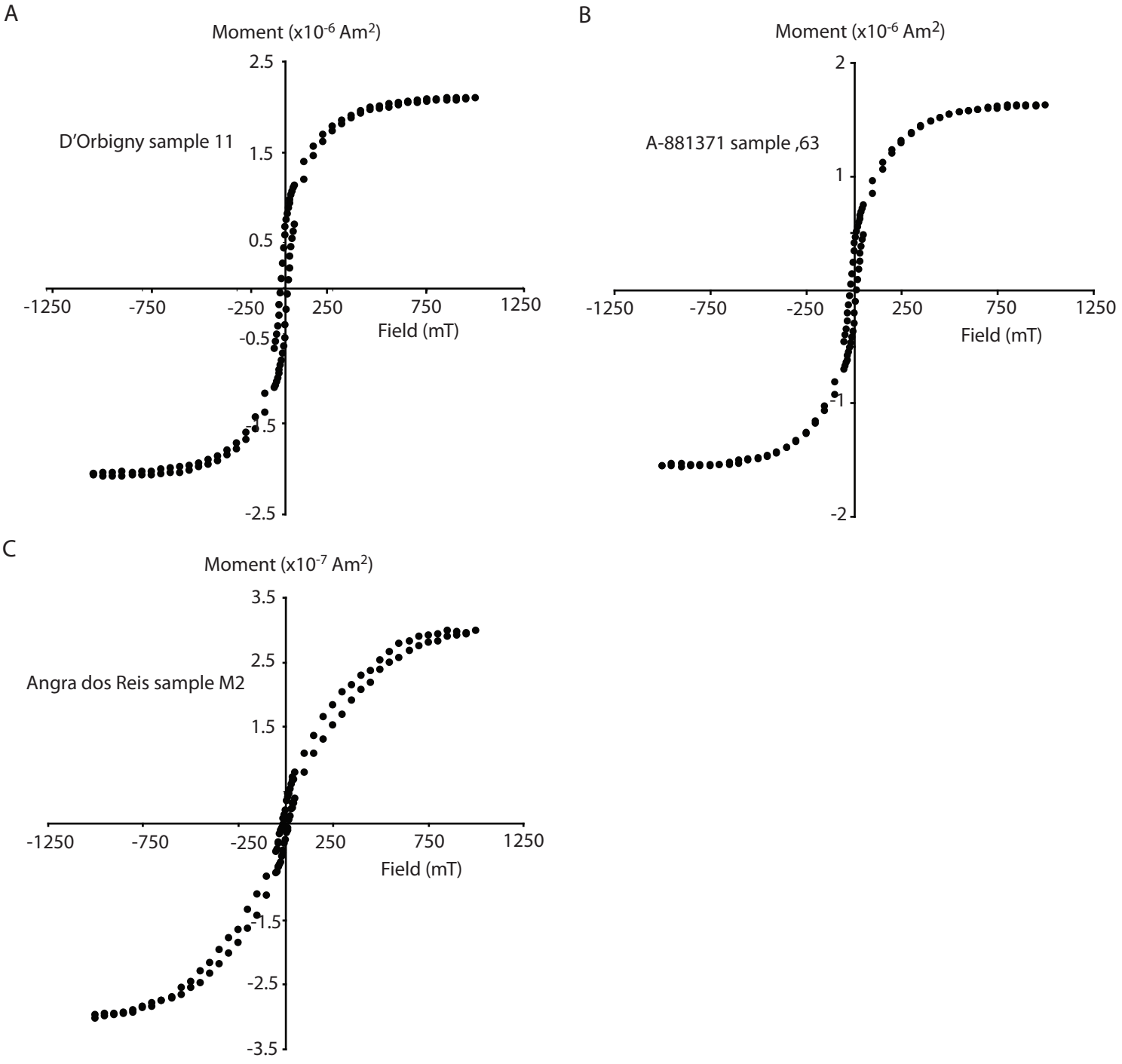

Weiss et al. 2008 Figure S4

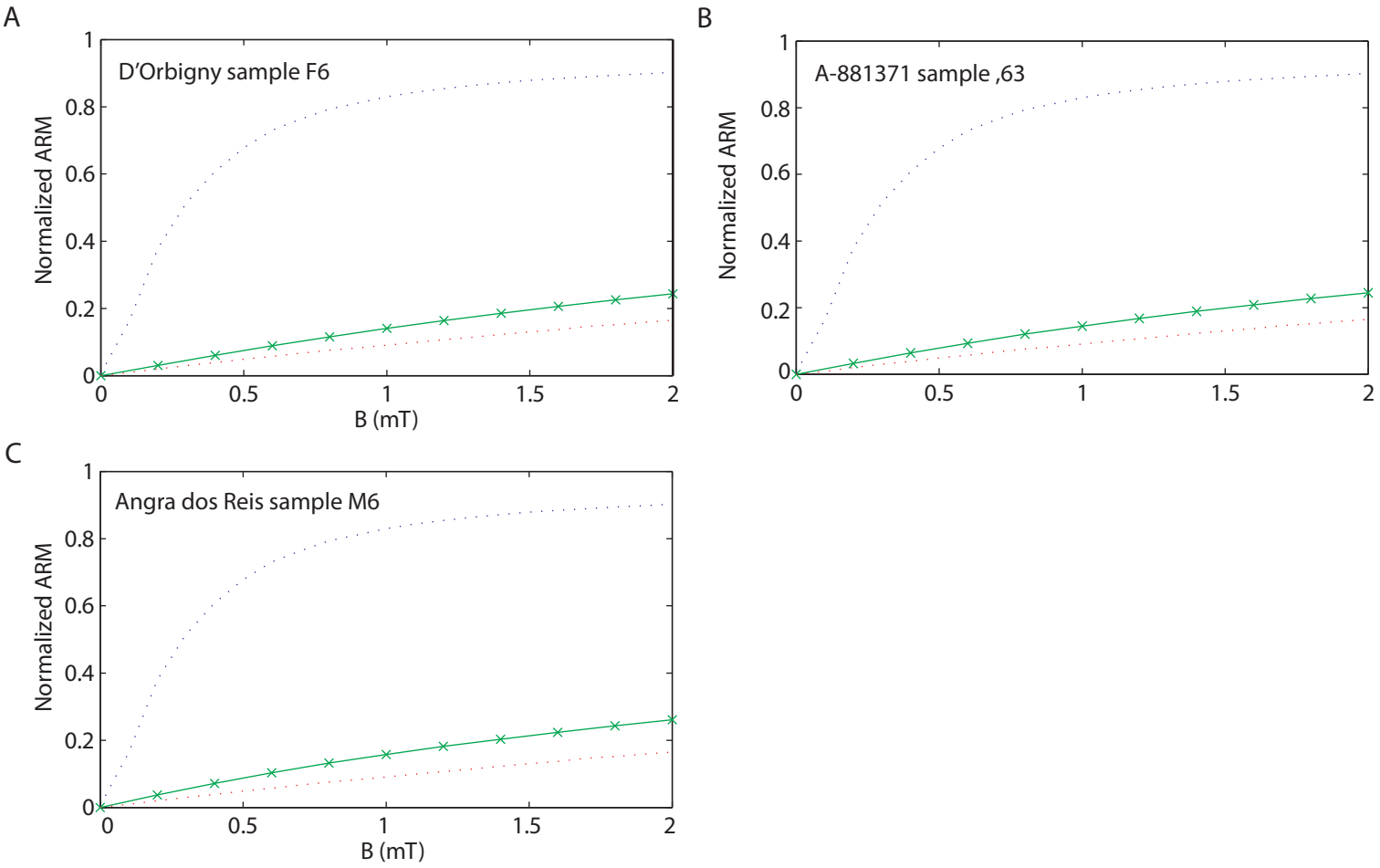

Weiss et al. 2008 Figure S5

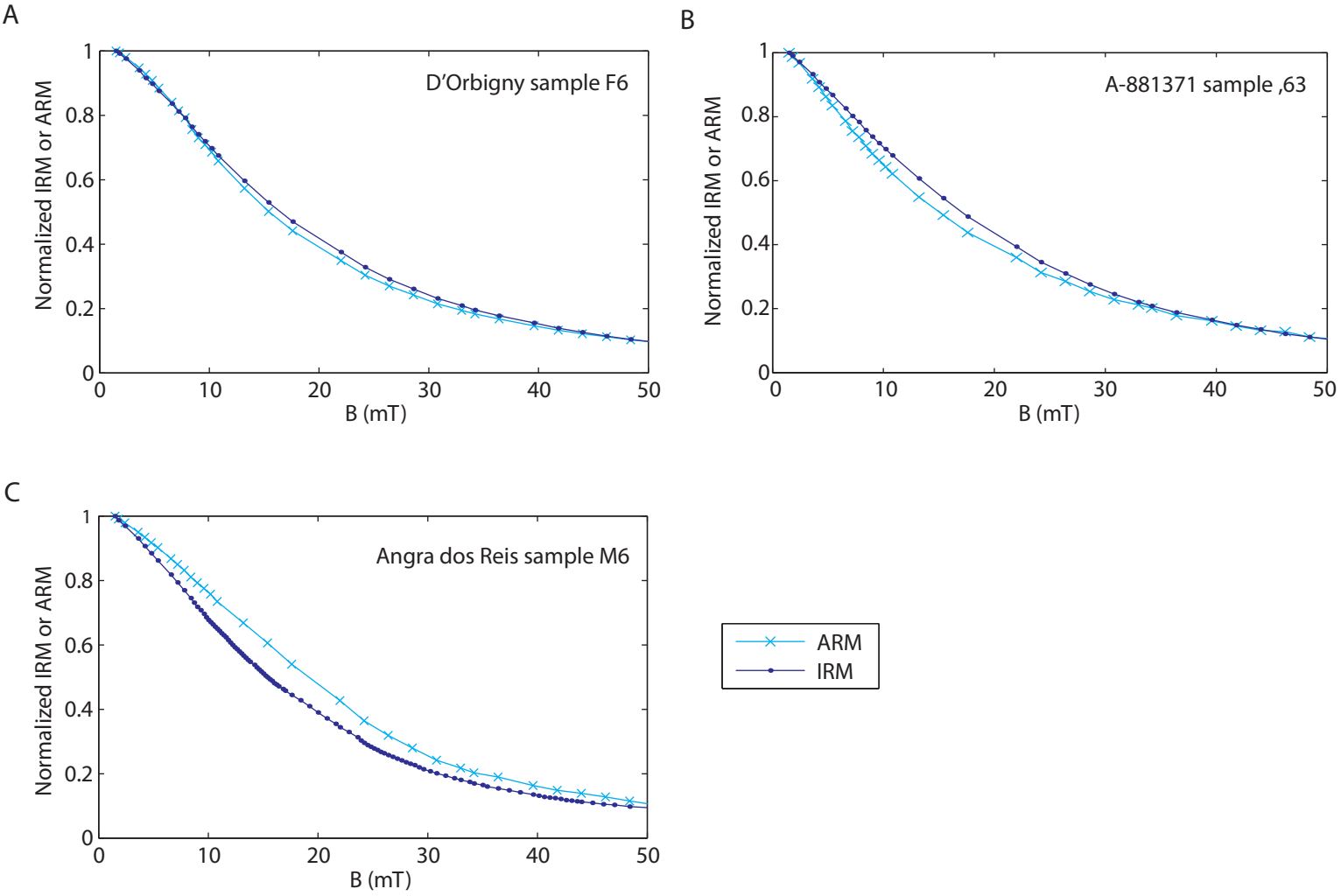

Weiss et al. 2008 Figure S6

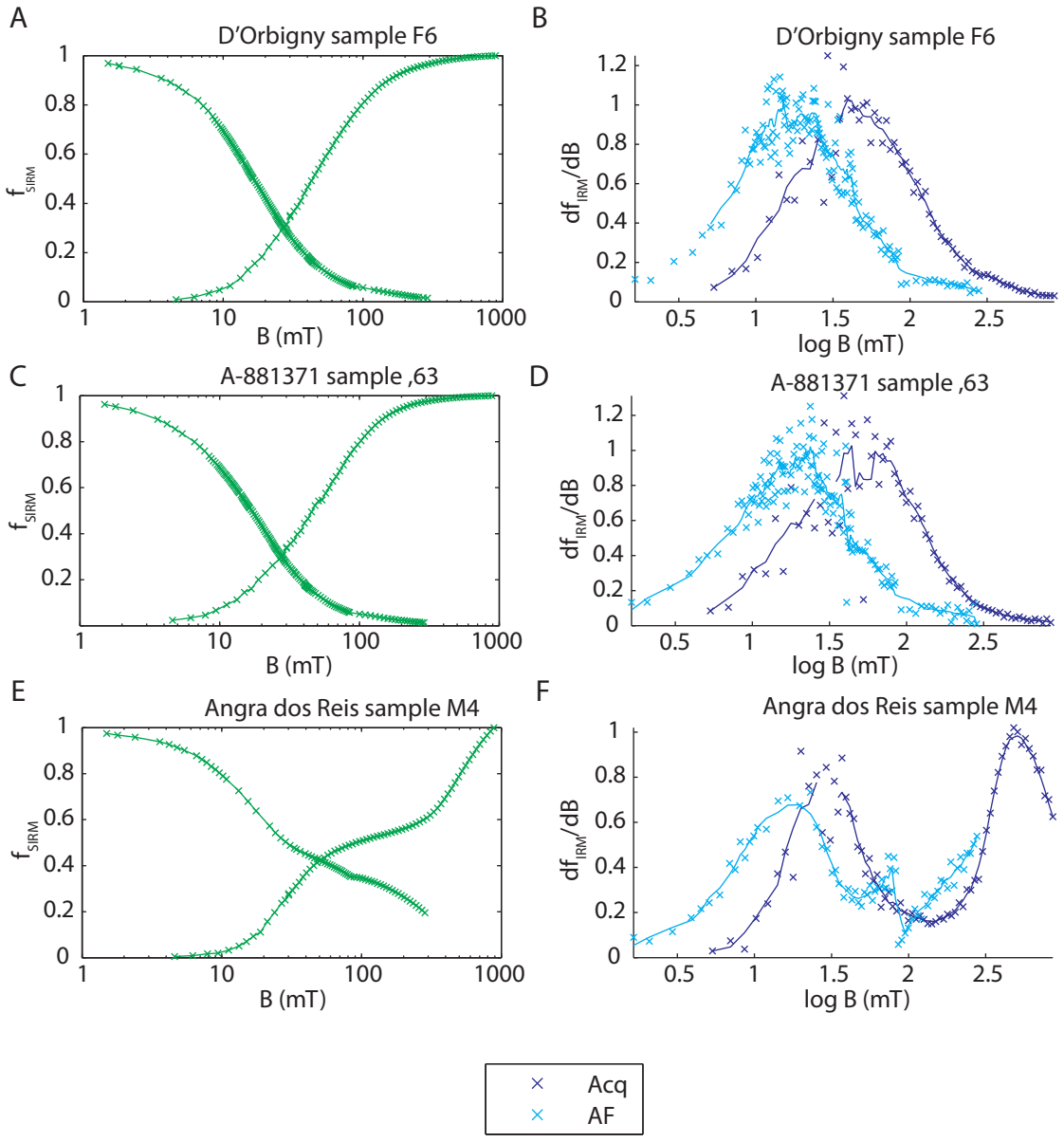

Weiss et al. 2008 Figure S7

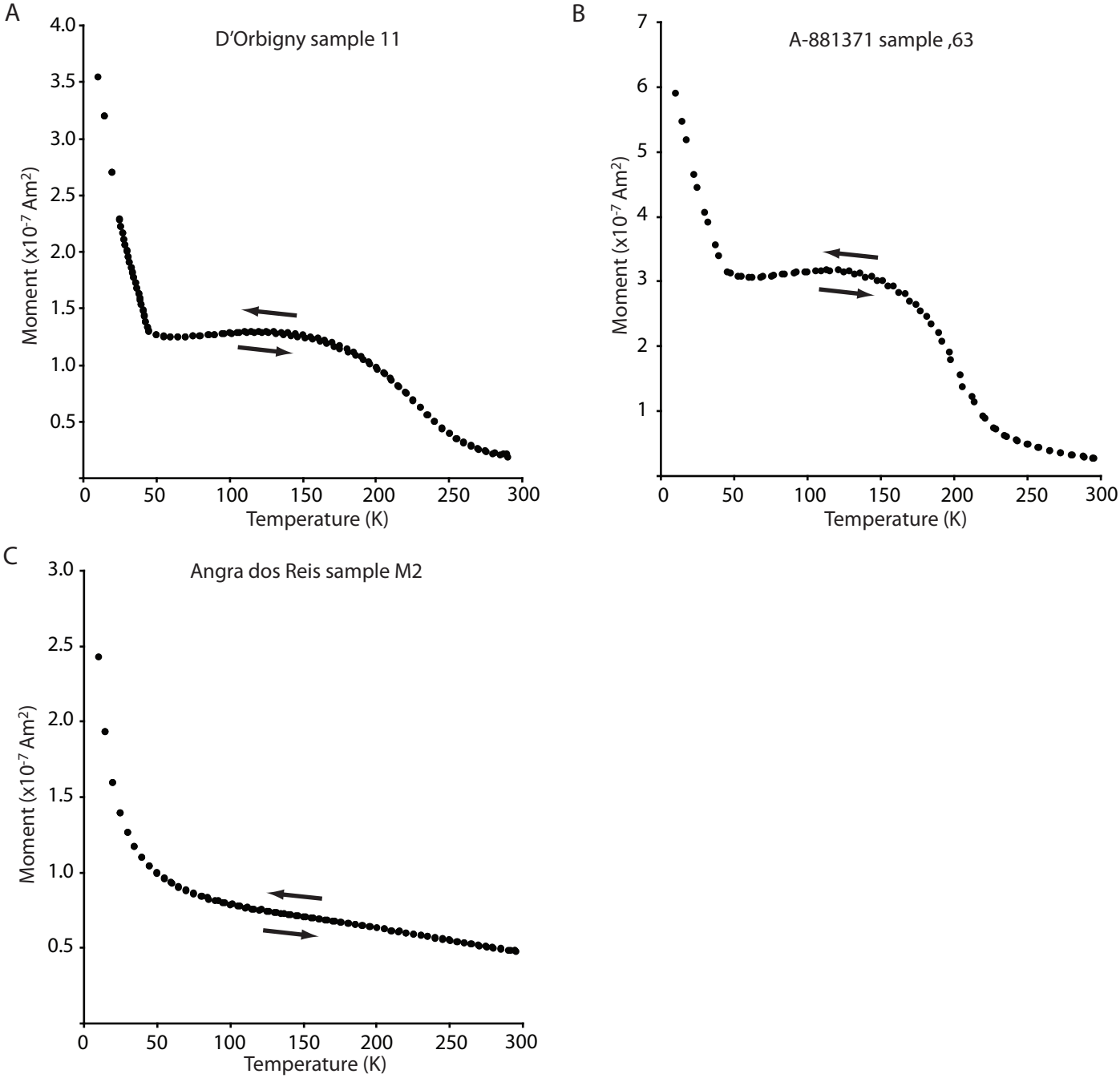

Weiss et al. 2008 Figure S8

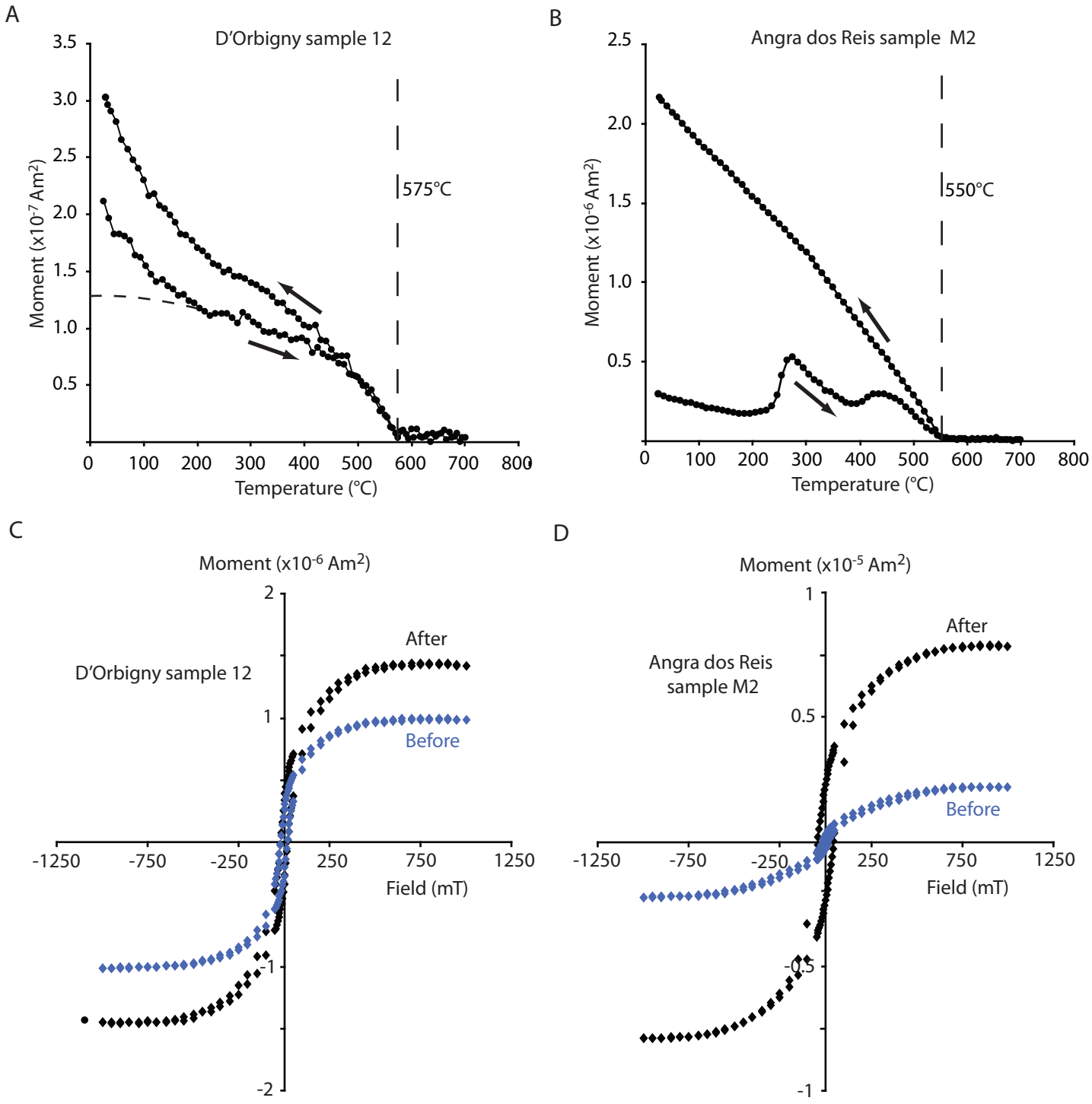

Weiss et al. 2008 Figure S9

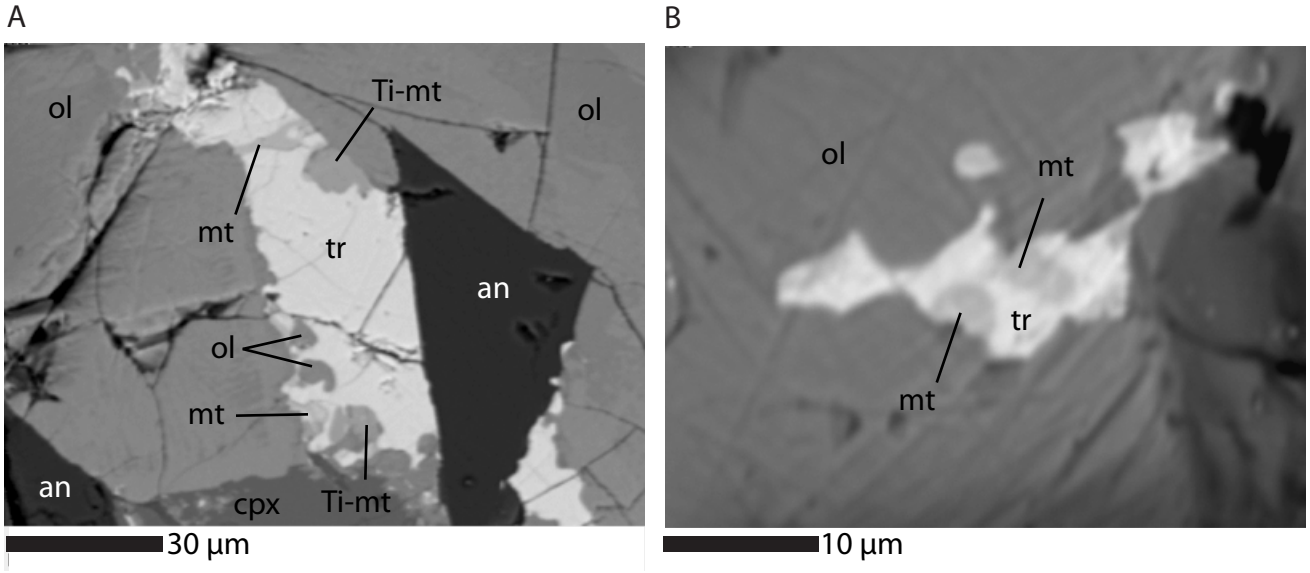

Weiss et al. 2008 Figure S10

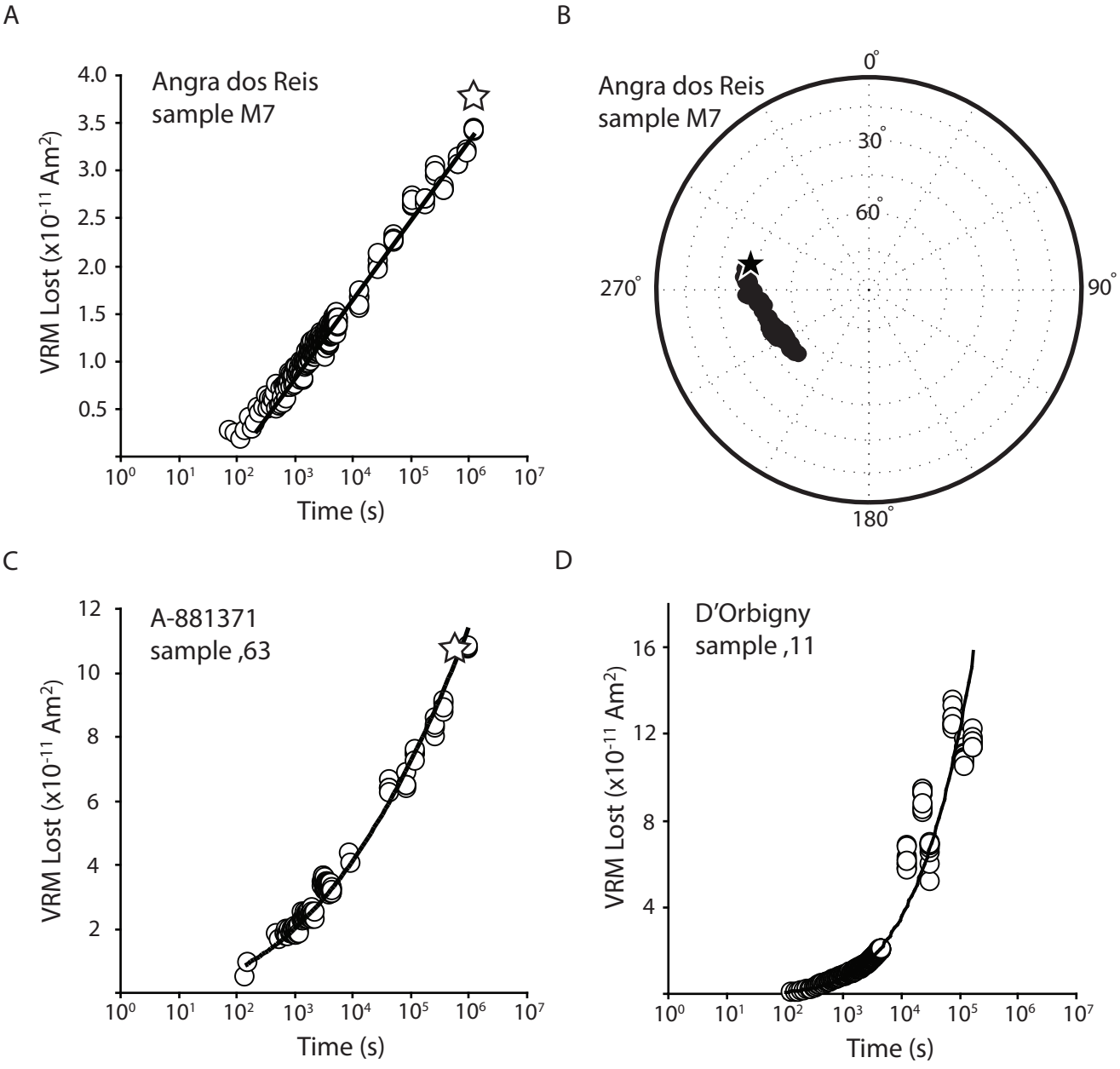

Weiss et al. 2008 Figure S11

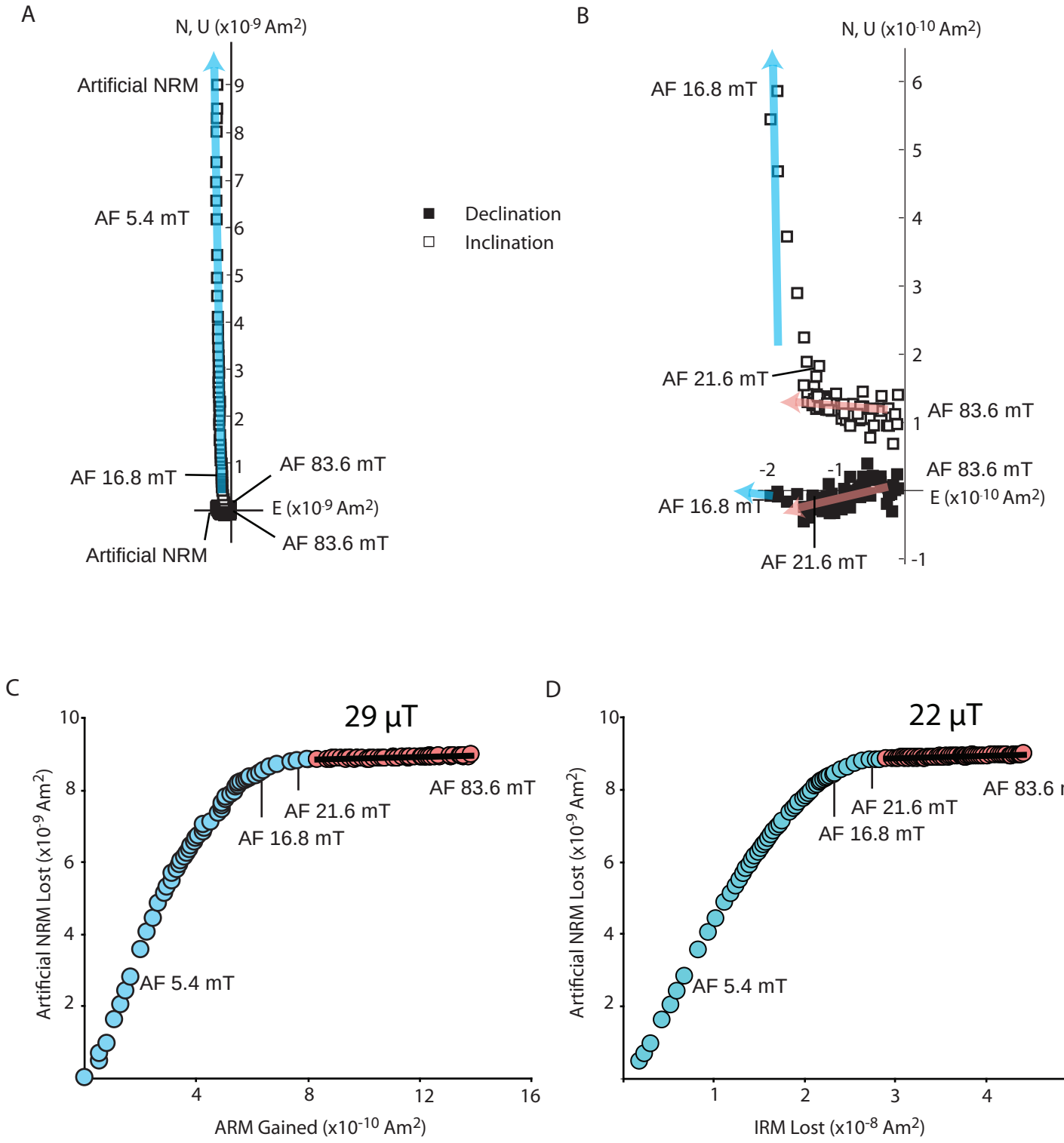

Weiss et al. 2008 Figure S12